Unsworth, M., Comeau, M.J., Diaz, D., Brasse, H., Heit, B., Favetto, A., Pomposiello, C., Barce-lona, H., Peri, G., and Ticona, F., 2023, Crustal structure of the Lazufre volcanic complex and the Southern Puna from 3-D inversion of magnetotelluric data: Implications for surface uplift and evidence for melt storage and hydrothermal fluids: Geosphere, v. 19, https://doi.org/10.1130/GES02506.1.

Supplementary material for "Crustal structure of the Lazufre volcanic complex and the Southern Puna from 3-D inversion of magnetotelluric data: implications for surface uplift and evidence for melt storage and hydrothermal fluids"

1. Magnetotelluric data

This section contains additional figures that illustrate the measured field data. The station names and locations are listed in Table S1.

Figure S1 shows both the real (in-phase) and imaginary (out-of-phase) components of the induction vectors. These vectors are computed from the vertical magnetic fields at each MT station. If the subsurface resistivity structure were 2-D, then the vectors would all be normal to the strike direction. At short periods (1-10 s) the direction of the arrows is quite scattered, indicating a 3-D resistivity structure. At a period of 100 s the arrows are less scattered, indicating a more 2-D structure that is parallel to the Salar de Antofalla.

Figure S2 shows the phase tensors at periods of 1 s, 10 s and 100 s. As period increases, the depth of penetration in the Earth increases. The strike direction is close to the major or minor axis of the ellipse, and the rose diagram shows the statistical distribution of the major axis directions. At a period of 1 s, there is no dominant strike direction. At longer periods the signals penetrate deeper into the Earth and a strike in the range N30°E – N45°E is observed. The color filling shows the skew angle which is a measure of the 3-D nature of the impedance tensor.

Name	Collected by	Latitude (°S)	Longitude (°W)	Elevation (m)
1463N12_13	Univ. of Alberta	25.652	66.850	4120
1463N14_13	Univ. of Alberta	25.528	66.951	4120
1463O18_13	Univ. of Alberta	25.516	67.591	3320
1463O19_13	Univ. of Alberta	25.595	67.404	4620
1463O20_13	Univ. of Alberta	25.517	67.209	4120
1463O21_13	Univ. of Alberta	25.552	67.551	3320
1463O22_13	Univ. of Alberta	25.340	67.906	4020
1463O23_13	Univ. of Alberta	25.337	67.874	4020
1463O24_13	Univ. of Alberta	25.288	68.082	3720
1465N12_13	Univ. of Alberta	25.657	66.803	4120
1465N13_13	Univ. of Alberta	25.747	66.711	4120
1465N14_13	Univ. of Alberta	25.512	67.036	4420
1465O18_13	Univ. of Alberta	25.617	67.504	4120
1465O19_13	Univ. of Alberta	25.540	67.324	4020
1465O20_13	Univ. of Alberta	25.532	67.274	4020
1465O21_13	Univ. of Alberta	25.439	67.615	4020
1465O22_13	Univ. of Alberta	25.308	67.710	4120
1465O23_13	Univ. of Alberta	25.305	67.769	4120
1465O24_13	Univ. of Alberta	25.276	68.216	4120
1465O25_13	Univ. of Alberta	25.299	68.139	3920
1493O19_13	Univ. of Alberta	25.599	67.455	4120
1493O20_13	Univ. of Alberta	25.466	67.164	3920
1493O21_13	Univ. of Alberta	25.405	67.672	4120
1493O22_13	Univ. of Alberta	25.296	67.819	4320
1493O23_13	Univ. of Alberta	25.344	68.005	4220
1493O24_13	Univ. of Alberta	25.267	68.328	4320
1493O25_13	Univ. of Alberta	25.152	68.447	4820
1494N12_13	Univ. of Alberta	25.576	66.919	4220
1494N13_13	Univ. of Alberta	25.732	66.763	4220
1494N14_13	Univ. of Alberta	25.510	66.999	4220
1494O19_13	Univ. of Alberta	25.578	67.366	4520
1494O20_13	Univ. of Alberta	25.467	67.131	4120
1494O22_13	Univ. of Alberta	25.485	67.618	3520
1494O23_13	Univ. of Alberta	25.339	67.960	4020
1494O24_13	Univ. of Alberta	25.266	68.289	4320
1494O25_13	Univ. of Alberta	25.306	68.049	3720
A01	Freie Univ. Berlin	25.283	68.491	4920
A04	Freie Univ. Berlin	25.327	68.718	3820
L01	Freie Univ. Berlin	25.046	68.574	3920
L02	Freie Univ. Berlin	25.129	68.710	3620
L03	Freie Univ. Berlin	25.236	68.853	3520

L04	Freie Univ. Berlin	25.225	68.996	3820
L05	Freie Univ. Berlin	25.110	68.481	4720
L06	Freie Univ. Berlin	25.228	68.448	4520
L07	Freie Univ. Berlin	25.264	68.370	4320
L08	Freie Univ. Berlin	25.222	69.109	3920
L09	Freie Univ. Berlin	25.272	68.251	4320
L10	Freie Univ. Berlin	25.267	68.177	4020
L14	Freie Univ. Berlin	25.485	68.709	4320
L15	Freie Univ. Berlin	25.464	68.651	4120
e04	Universidad de Chile	25.154	68.542	4720
e10	Universidad de Chile	25.122	68.498	4520
e12	Universidad de Chile	25.126	68.580	4320
e14	Universidad de Chile	25.203	68.434	4420
e15	Universidad de Chile	25.221	68.409	4420
e16	Universidad de Chile	25.240	68.382	4320
e17	Universidad de Chile	25.259	68.354	4220
e18	Universidad de Chile	25.190	68.458	4620
e19	Universidad de Chile	25.133	68.468	5020
e20	Universidad de Chile	25.181	68.524	5120
e22	Universidad de Chile	25.160	68.524	5020
e23	Universidad de Chile	25.136	68.552	4420
e24	Universidad de Chile	25.139	68.515	4720
e26	Universidad de Chile	25.123	68.520	4420

Table S1 : Station names and locations for the MT stations used in the 3-D inversions. Note the elevations shown are those used in the modelling, which have been adjusted to fit the 100 m discretized vertical grid size for topography. They range from 3320 m to 5120 m with an average of 4210 m.

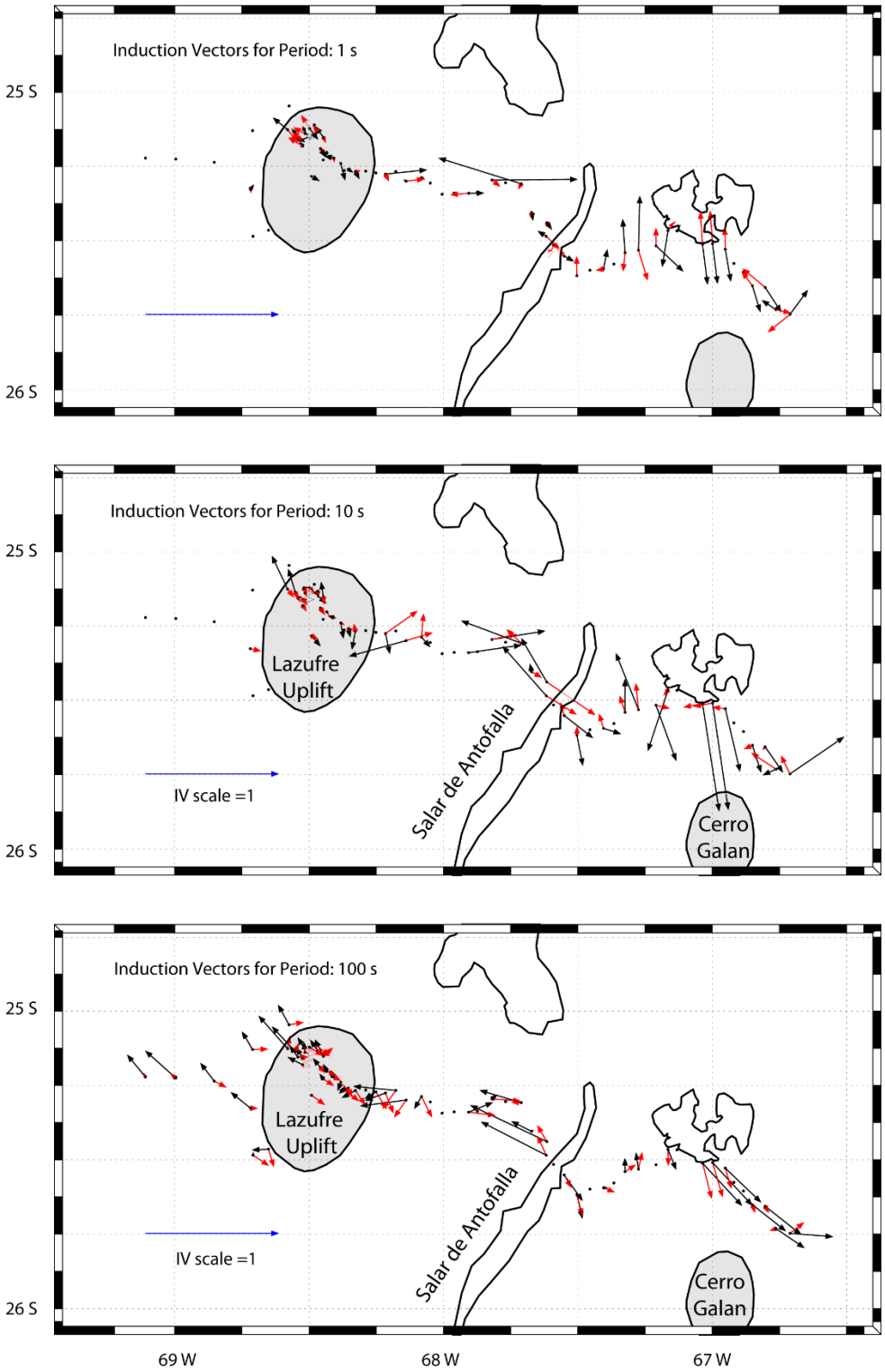

Figure S1 : Real (black) and imaginary (red) components of the induction vectors for the Puna MT profile.

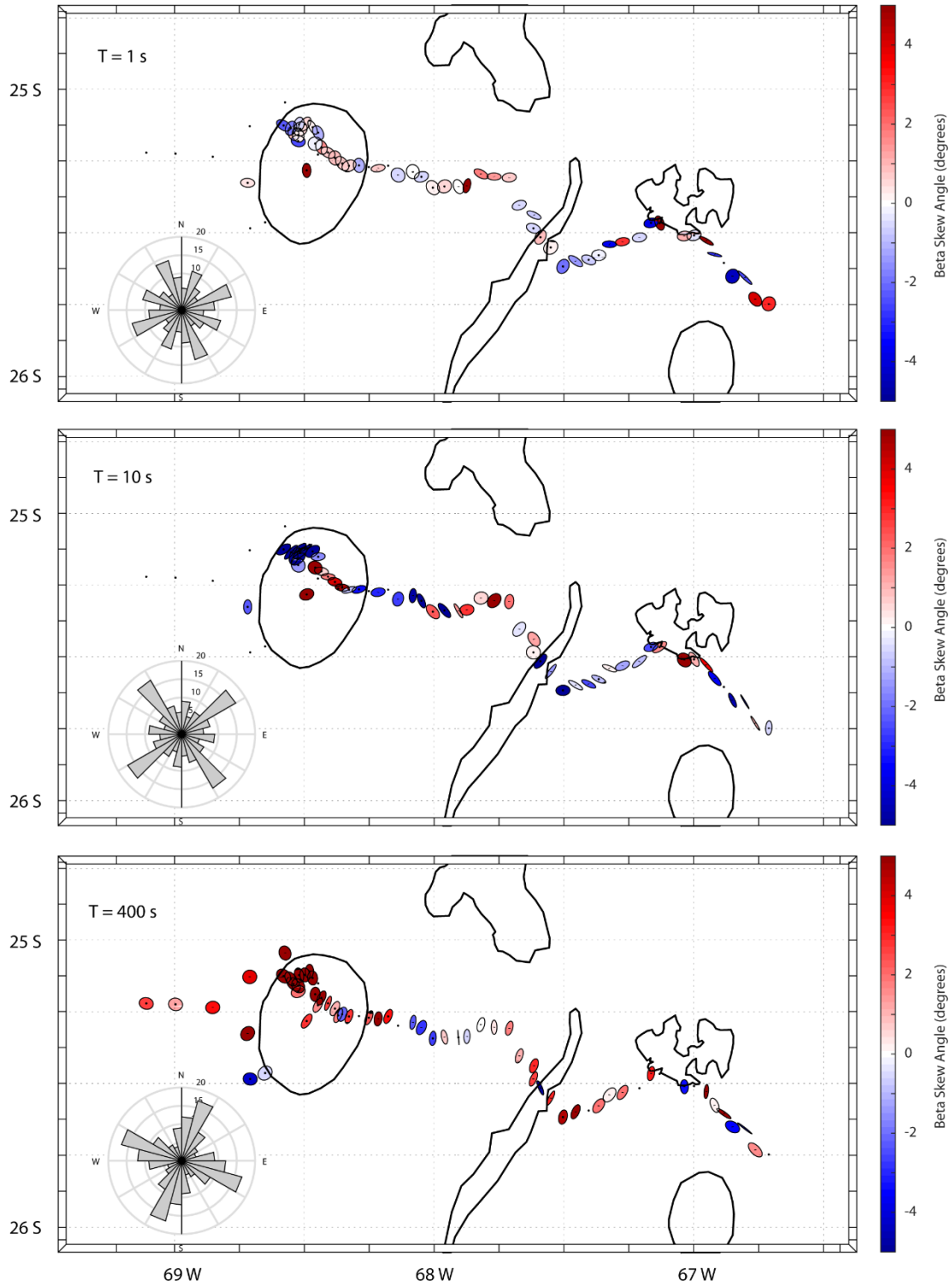

Figure S2 : Phase tensors for the Puna MT profile. The inset rose diagrams show the azimuthal distribution of the major axes of the phase tensor ellipses. See the text for a description of the phase tensors.

2. Forward responses of selected 3-D inversion models

In Figure S3 the predicted responses of the four inversion models are shown together for comparison as pseudosections of apparent resistivity, phase and tipper. The measured data are also shown for comparison. In Figure S4 the same responses are shown as residuals.

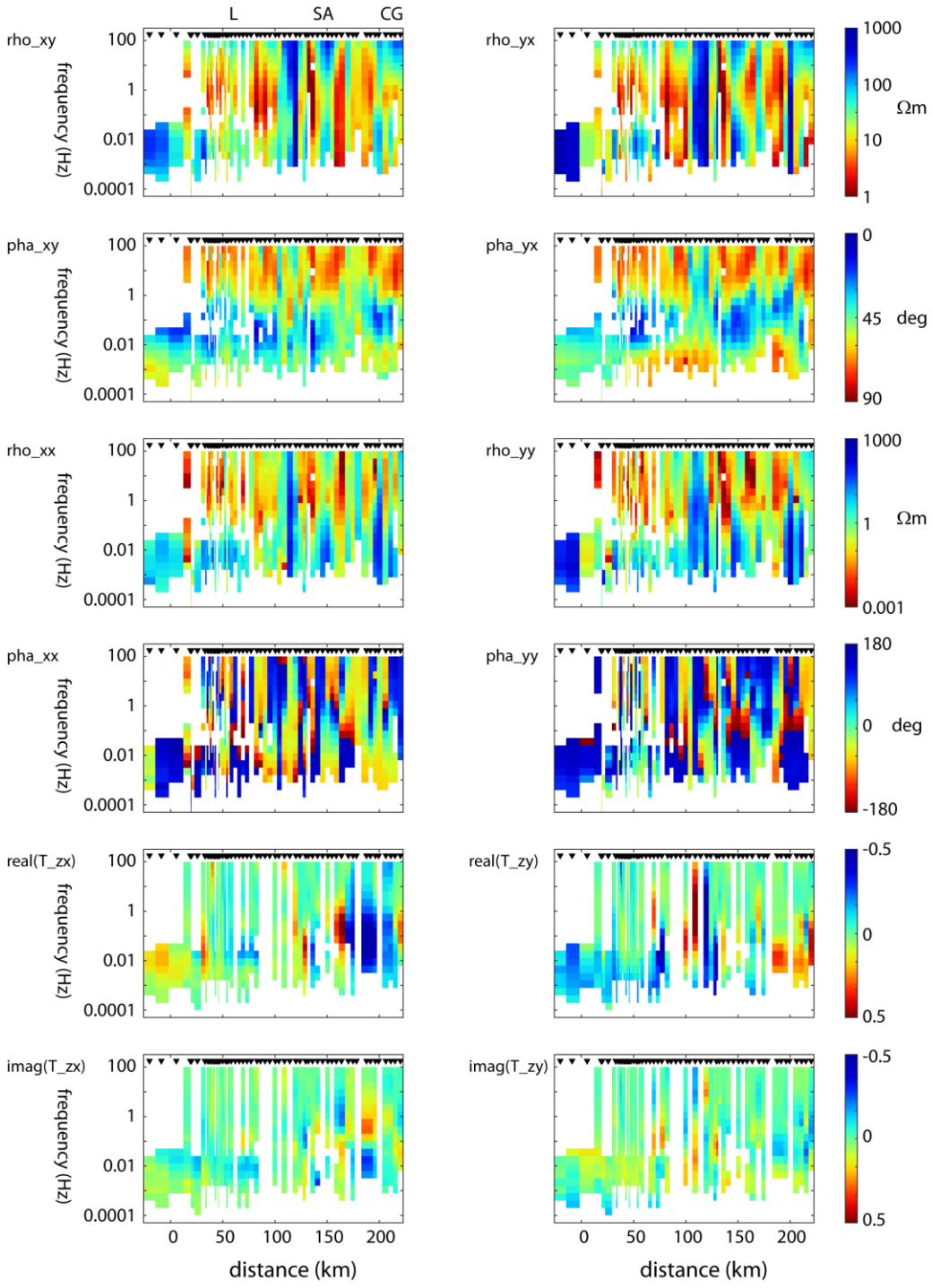

Figure S3(a) : Measured MT data (apparent resistivity, phase and tipper) in geographic co-ordinates. L = Lastarria, SA = Salar de Arizaro and CG = Cerro Galan.

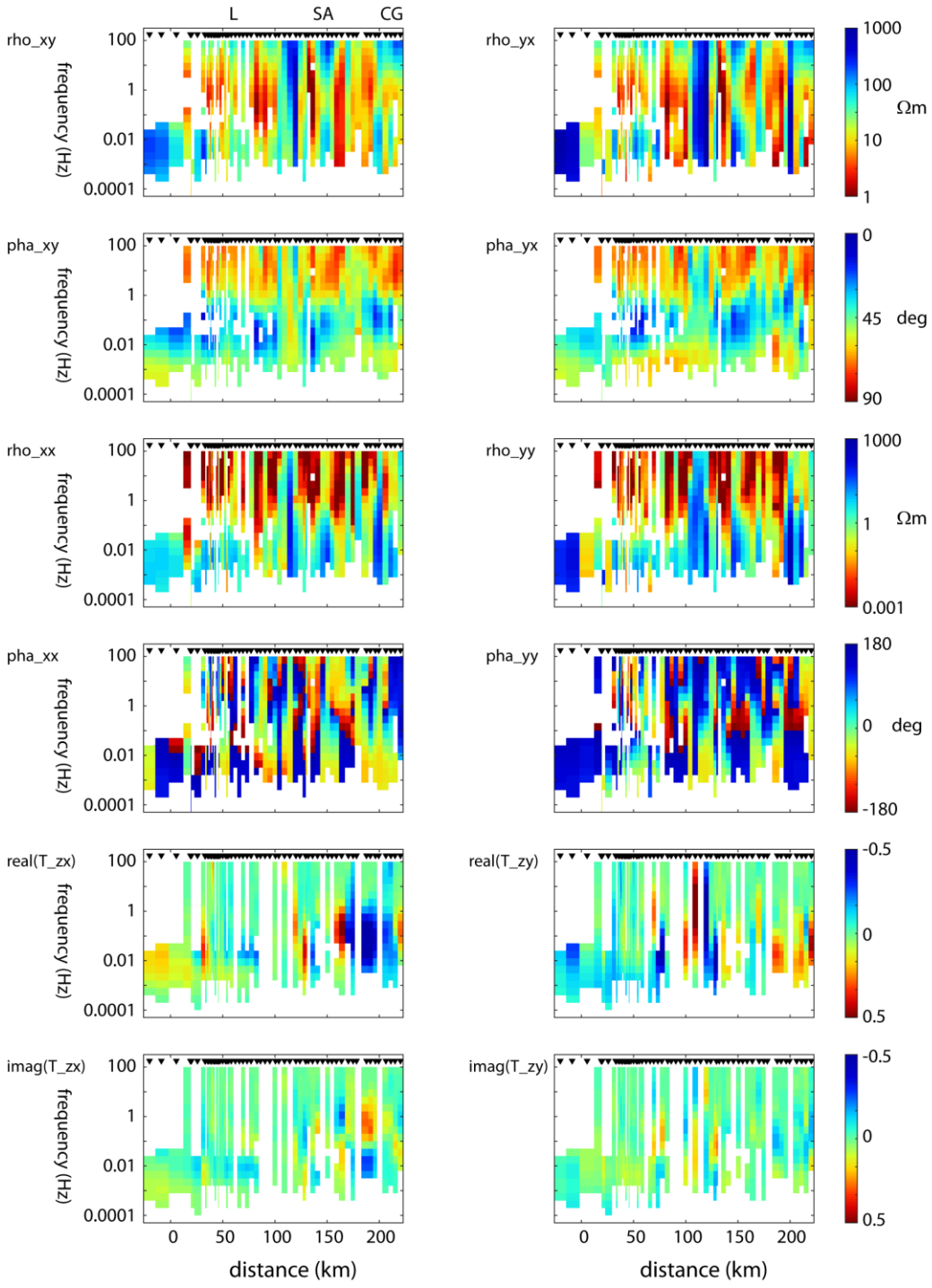

Figure S3(b) : Predicted MT data (apparent resistivity, phase and tipper) in geographic co-ordinates for inversion model *puna_lazufre_60a* shown in Figure 6.

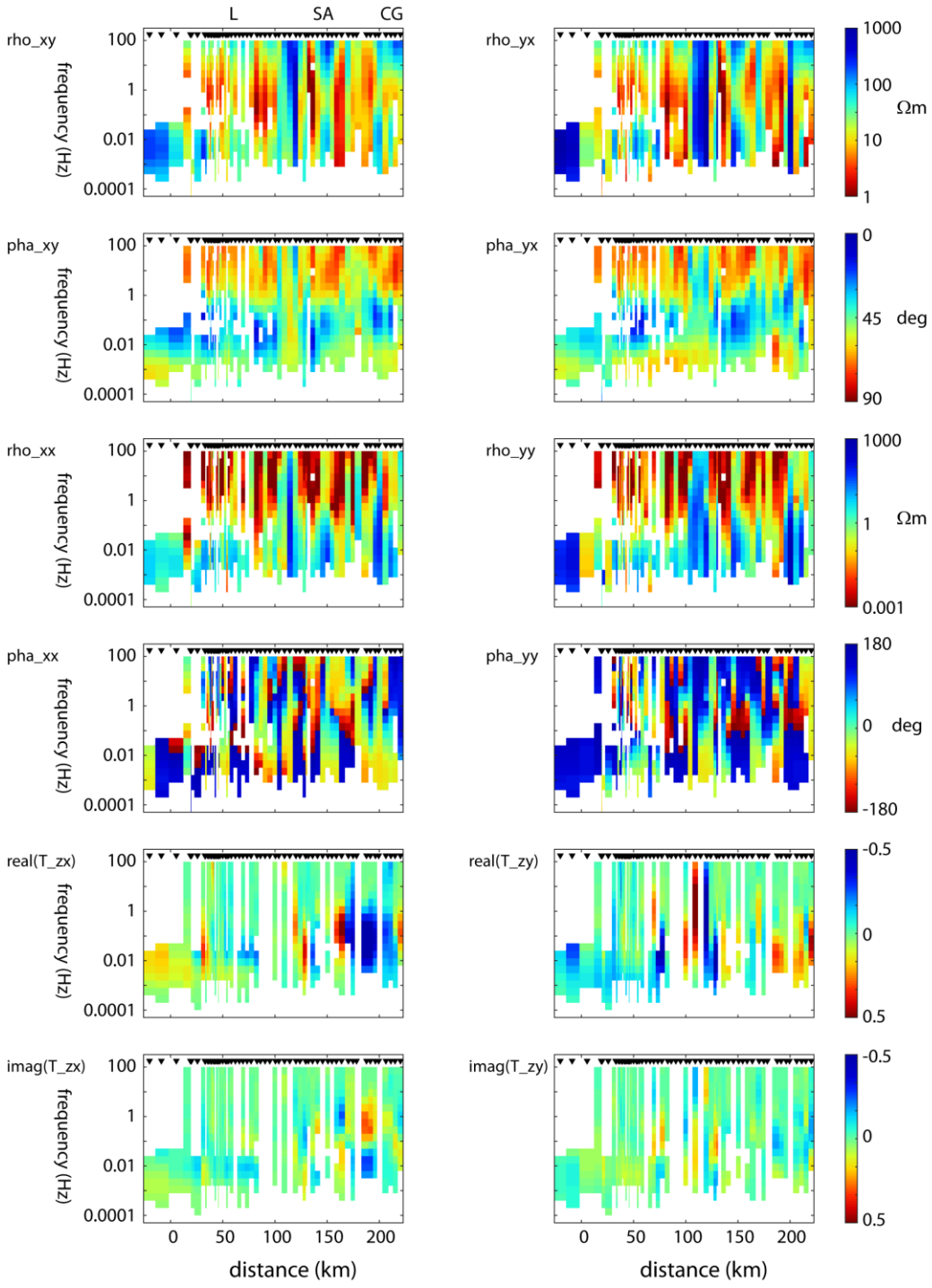

Figure S3(c) : Predicted MT data (apparent resistivity, phase and tipper) in geographic co-ordinates for inversion model *puna_lazufre_61c* shown in Figure 7.

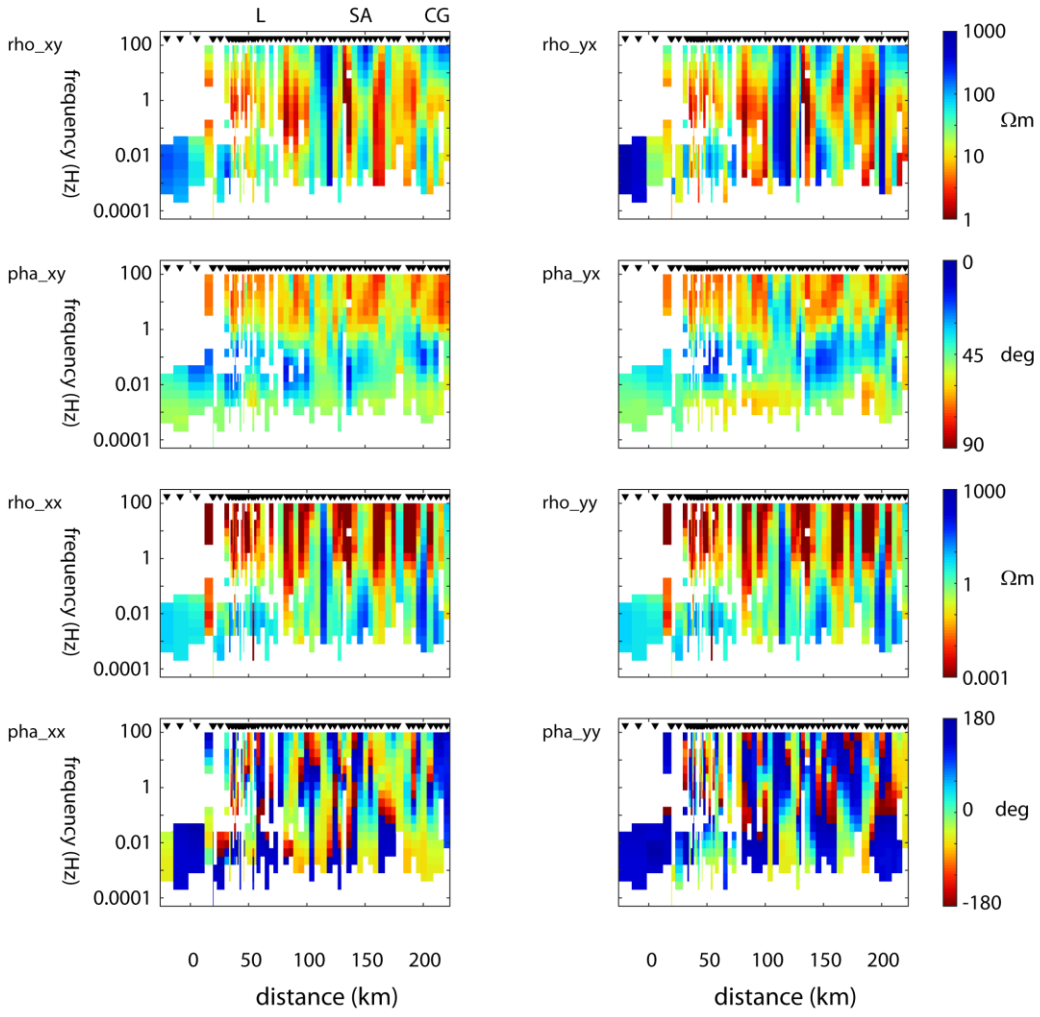

Figure S3(d) : Predicted MT data (apparent resistivity and phase) in geographic co-ordinates for inversion model *puna_lazufre_68a* obtained by inversion of impedance data only. Model is shown in Figure S5c.

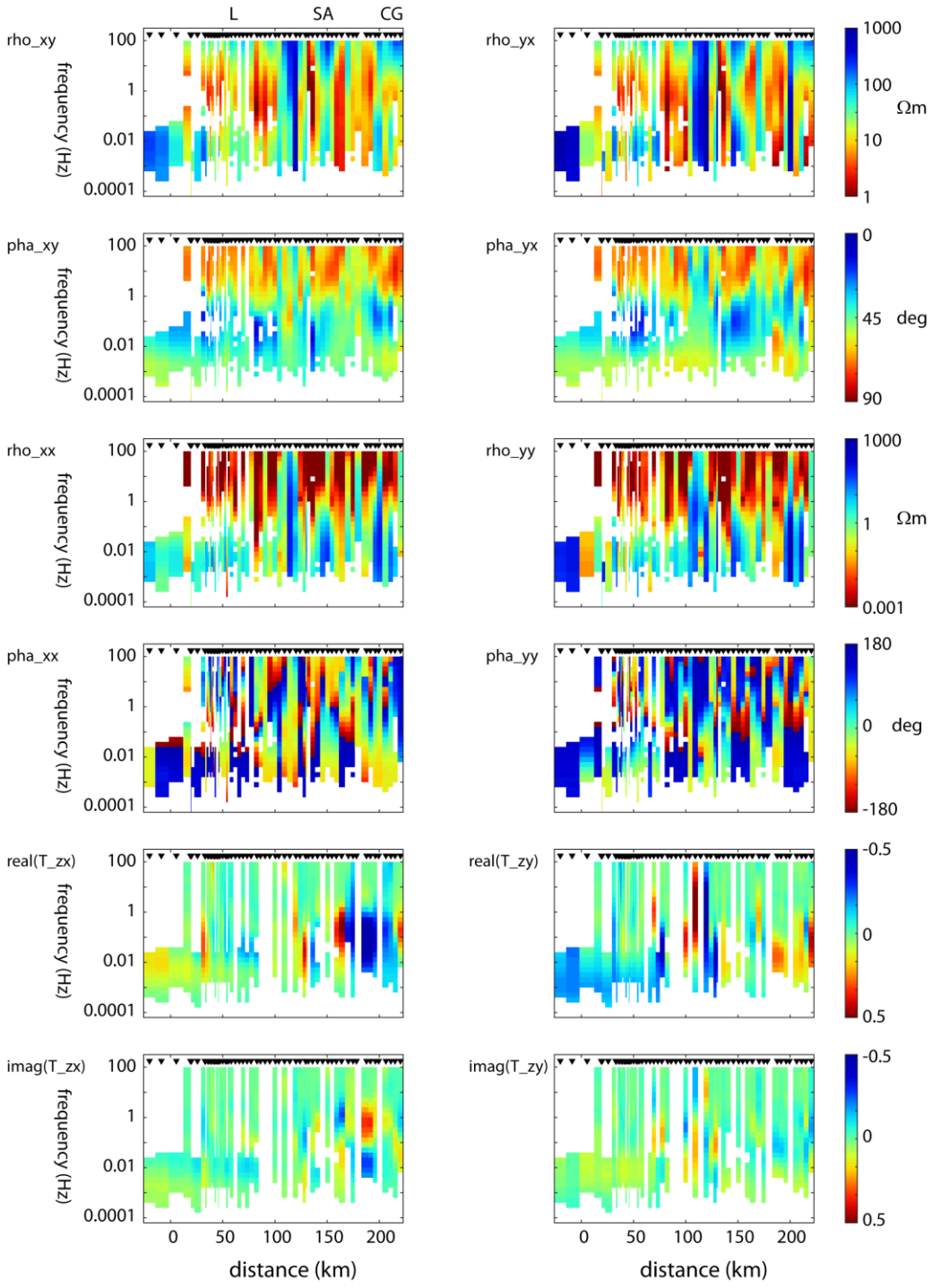

Figure S3(e) : Predicted MT data (apparent resistivity, phase and tipper) in geographic co-ordinates for inversion model *puna_lazufre_8a* shown in Figure S5d.

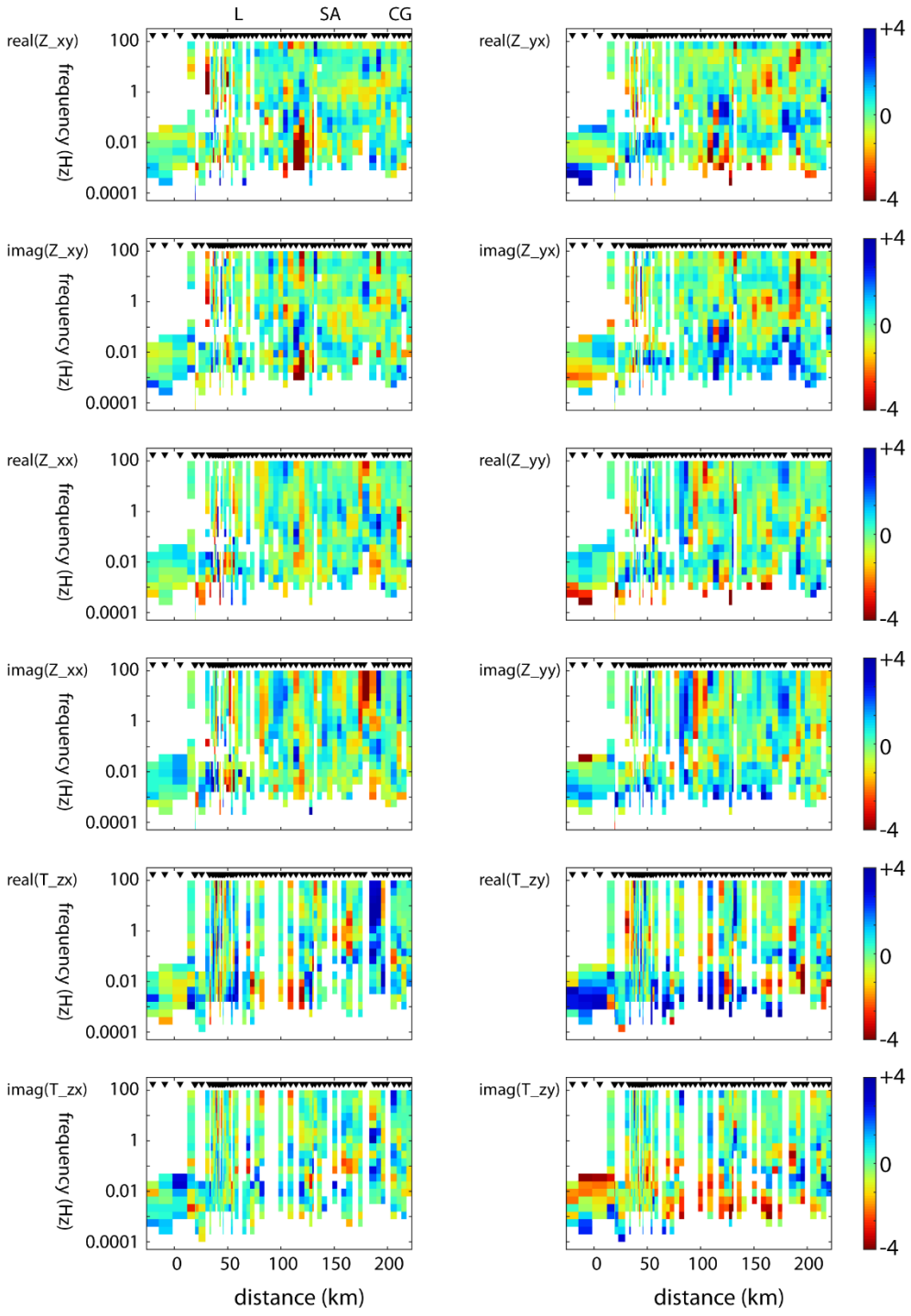

Figure S4(a) : Fit of predicted MT data (apparent resistivity, phase and tipper) in geographic co-ordinates for inversion model *puna_lazufre_60a* plotted as residuals.

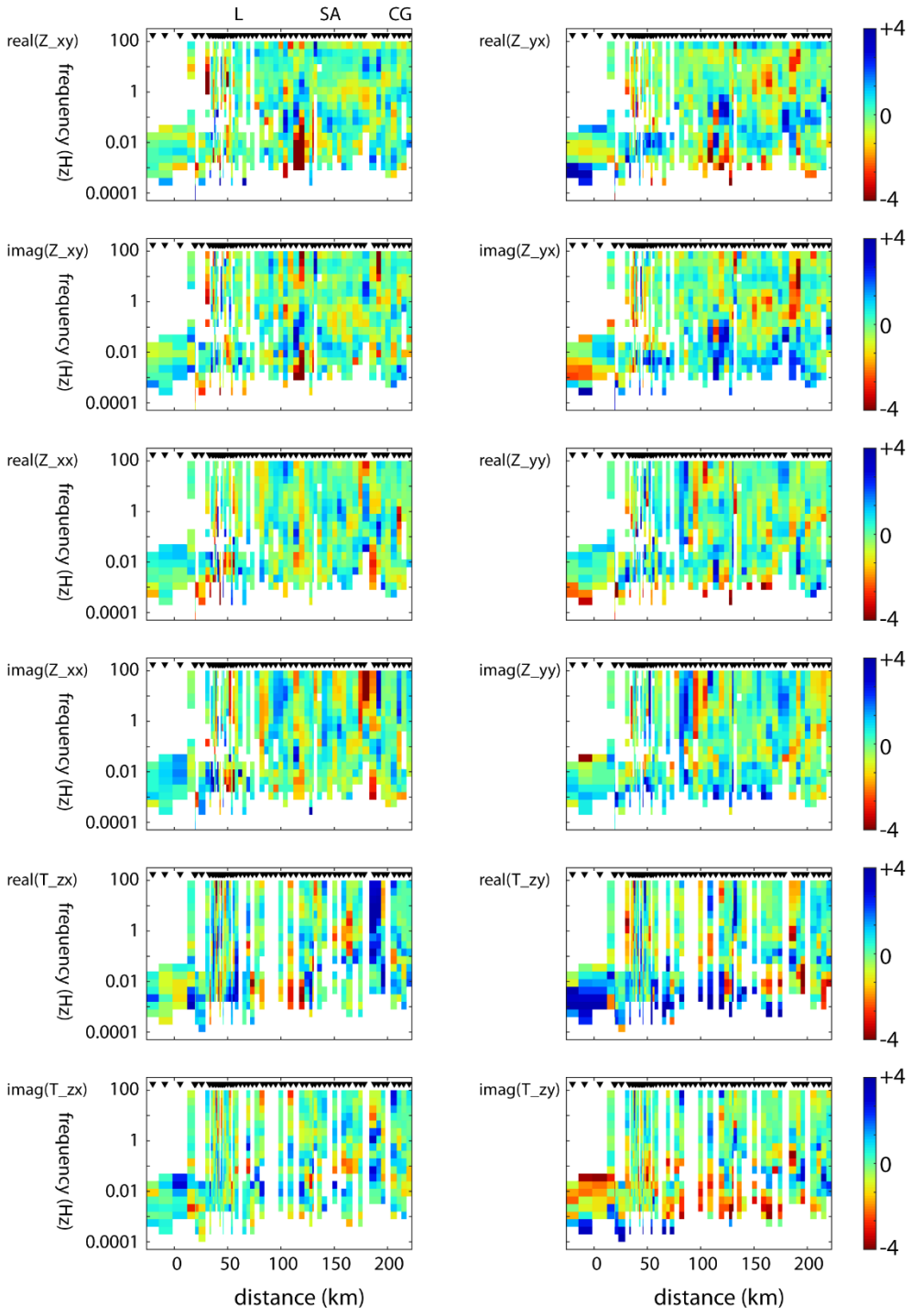

Figure S4(b) : Fit of predicted MT data (apparent resistivity, phase and tipper) in geographic co-ordinates for inversion model *puna_lazufre_61c* plotted as residuals.

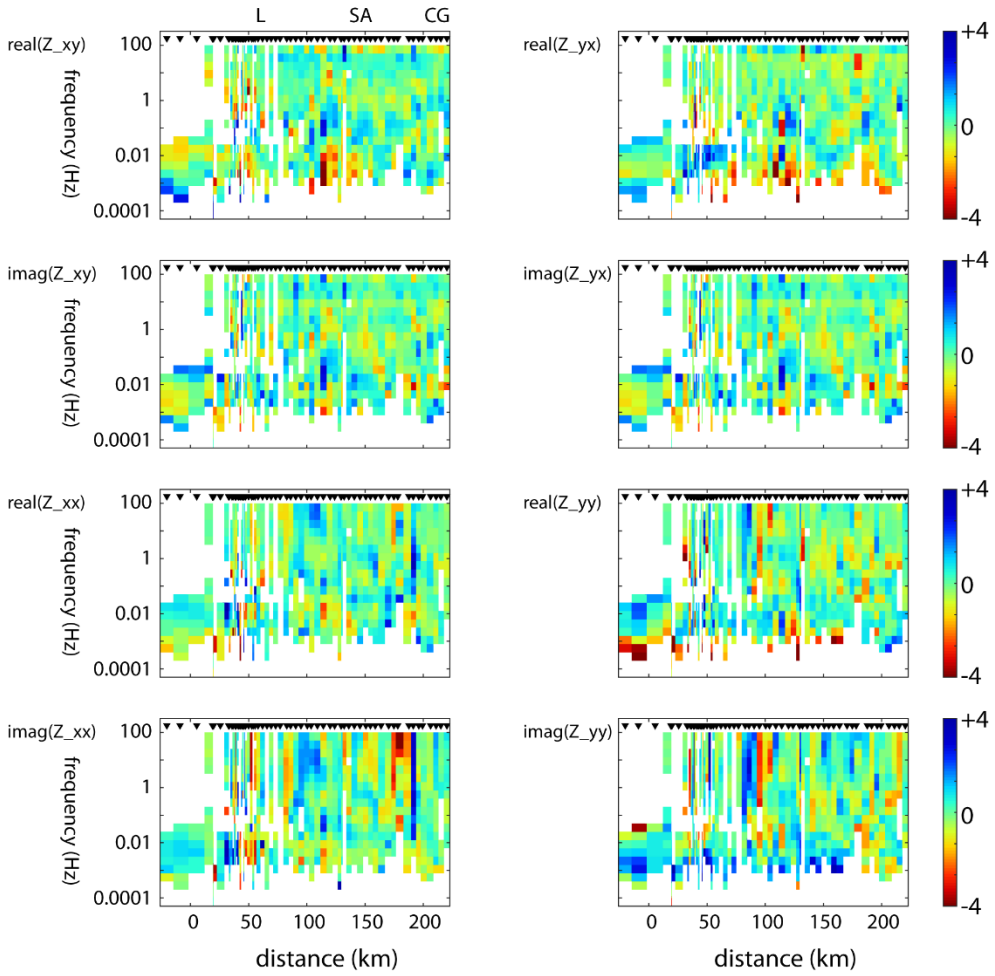

Figure S4(c) : Fit of predicted MT data (apparent resistivity and phase) in geographic co-ordinates for inversion model *puna_lazufre_68a* plotted as residuals.

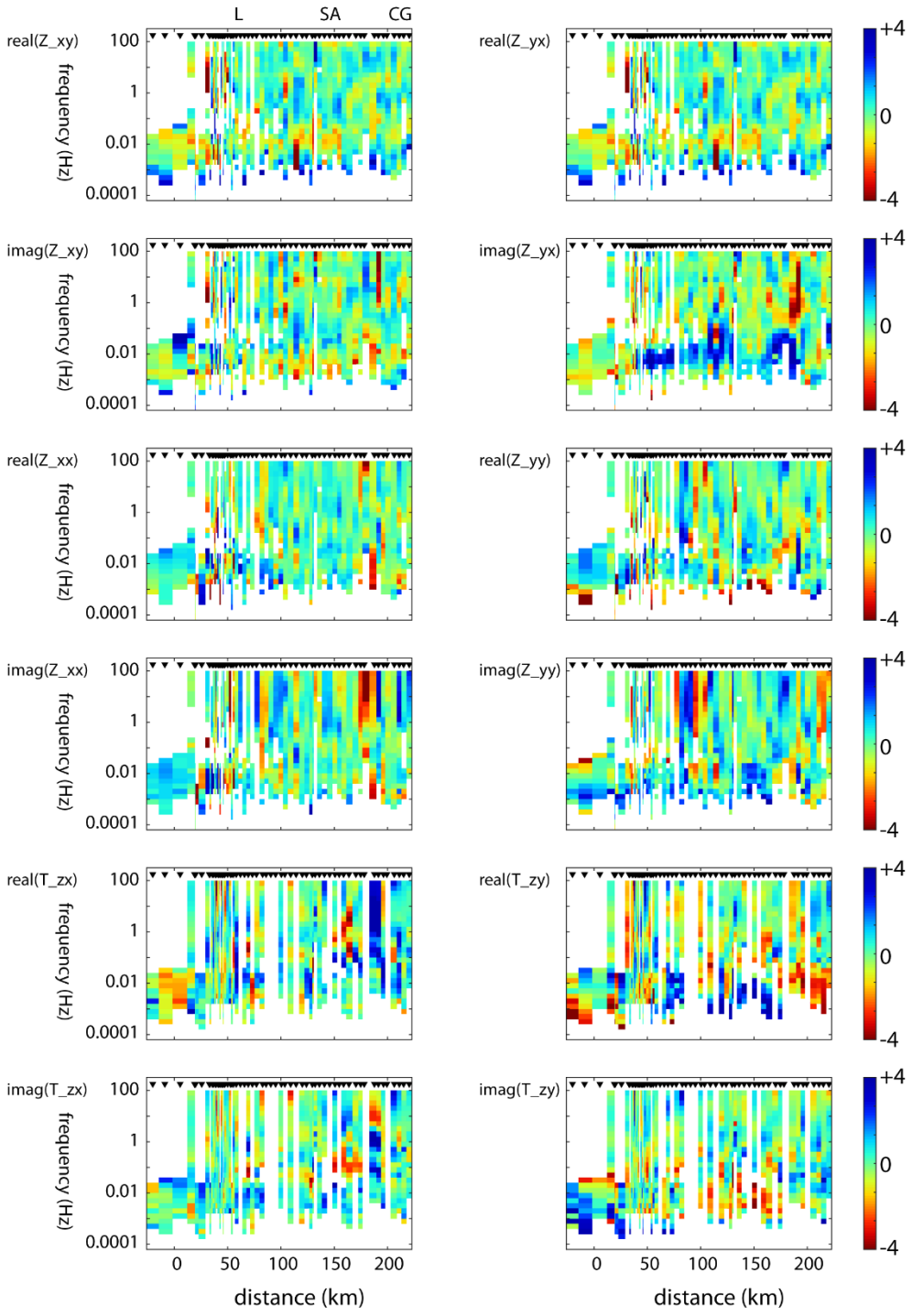

Figure S4(d) : Fit of predicted MT data (apparent resistivity, phase and tipper) in geographic co-ordinates for inversion model *puna_lazufre_68a* plotted as residuals.

3. Selected 3-D inversion models

Many individual inversions of the Puna MT data were performed. This section compares the four preferred models described in this paper.

	Inversion name	Data inverted	Starting model	Starting r.ms. misfit	Final r.ms. misfit	Iterations
Model-1 Figure 6	puna_lazufre_60a	Impedance + tipper	10 Ωm	7.50	1.60	207
Model-2 Figure 7	puna_lazufre_61c	Impedance + tipper	10 Ωm + 1000 Ωm Nazca plate	7.54	1.63	218
Model-3 Figure S5c	puna_lazufre_68a	Impedance	10 Ωm	7.99	1.42	173
Model-4 Figure S5d	puna_lazufre_8a	Impedance + tipper	100 Ωm	22.76	1.80	179

Table S2 : Summary of the four inversion models described in the Supplemental Material.

Figure S5 shows vertical and horizontal slices of these four models for comparison. As noted in the main text, it was found that the best fit was obtained when the starting model was a 10 Ωm halfspace. This allowed the inversion to place low resistivity regions in the lower crust and adjacent to Lazufre and Cerro Galan. This high sensitivity to the choice of starting model was not observed in other studies with the ModEM inversion when a grid of MT stations was used. It is possible that the higher resistivity starting model causes the inversion to become trapped in a local minimum. Our interpretation is that when a profile of stations, such as in this study, is inverted with a 3-D algorithm, the starting model exerts more influence because it imposes smoothing on the north and south edges of the model, in addition to the base. In the inversion of a grid of MT stations, the smoothing on the vertical edges will be reduced in comparison.

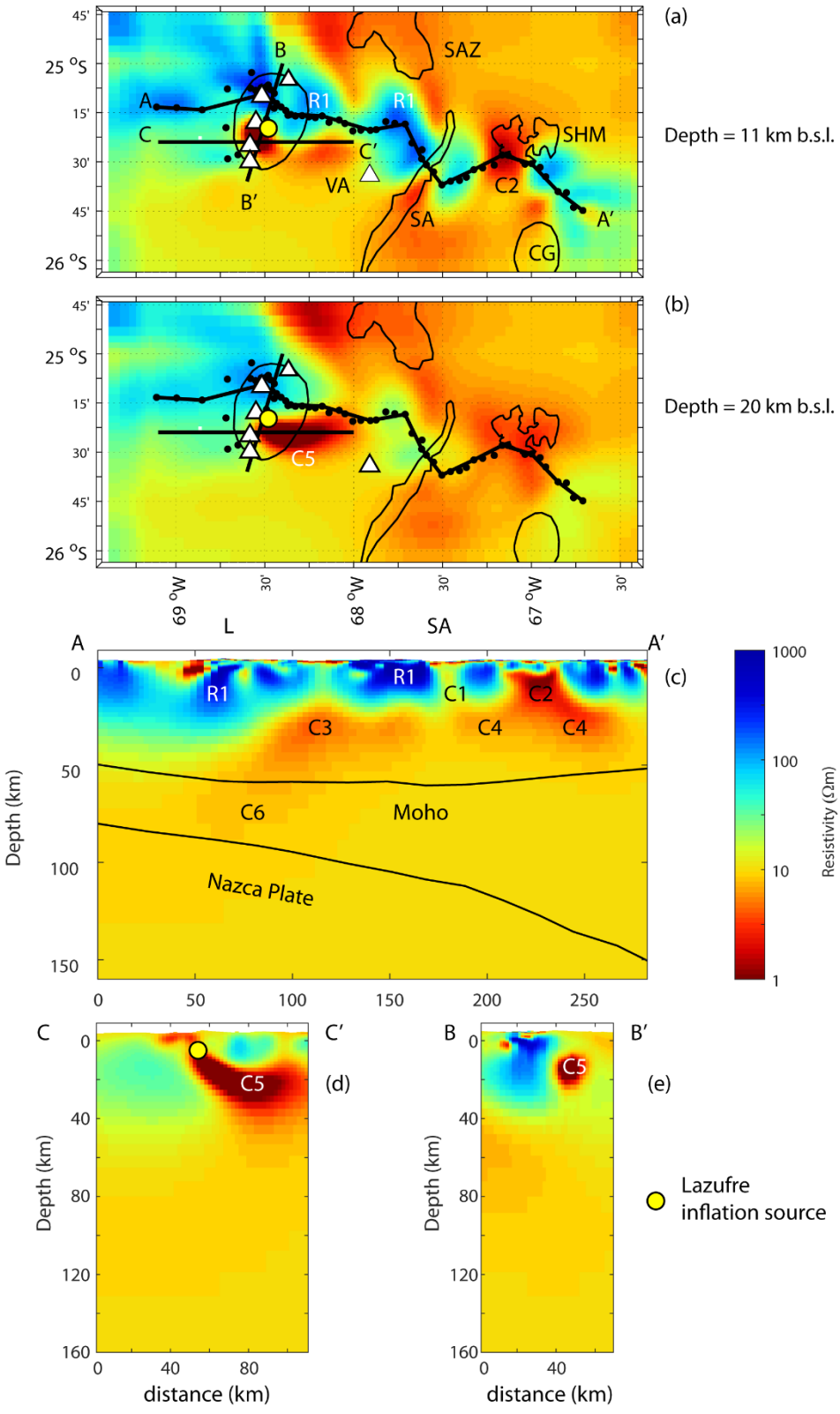

Figure S5(a) : Inversion model *puna_lazufre_60a* obtained by inversion of impedance and tipper data. Same model as in Figure 6 and shown here for comparison.

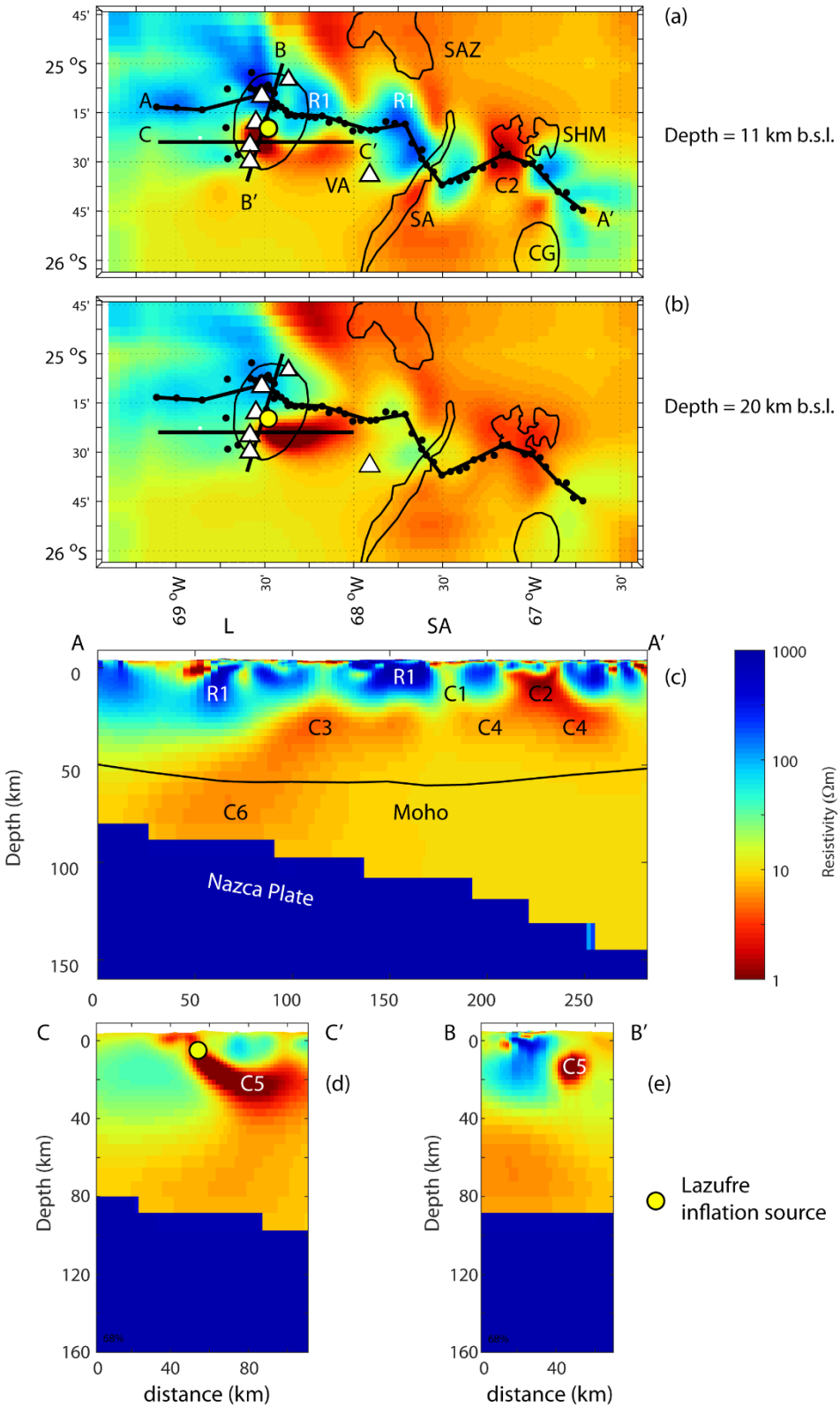

Figure S5(b) : Inversion model *puna_lazufre_61c* obtained by inversion of impedance and tipper data, starting from a model that represented the Nazca Plate as a resistor. Same as Figure 7.

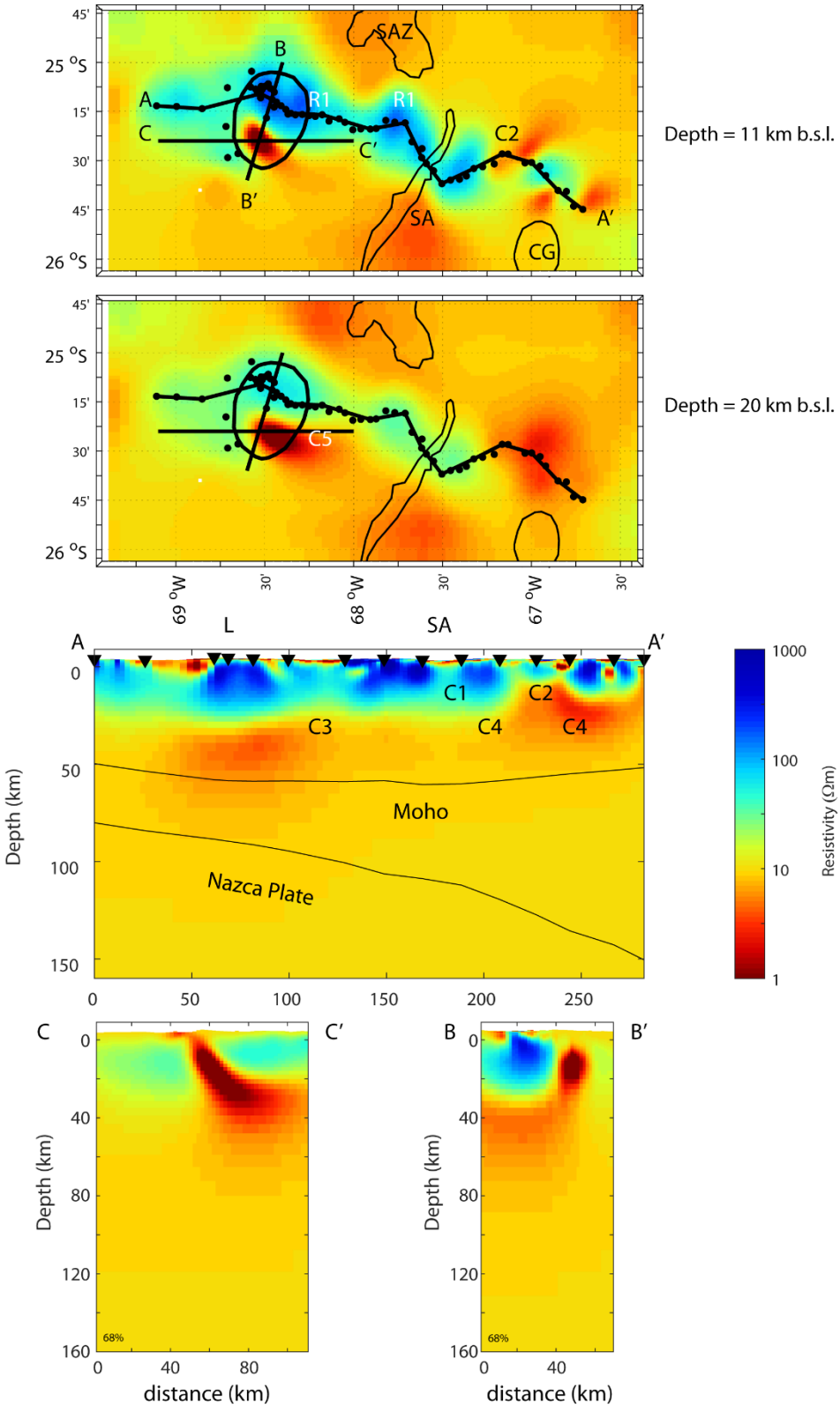

Figure S5(c) : Inversion model *puna_lazufre_68a* obtained by inversion of impedance data only.

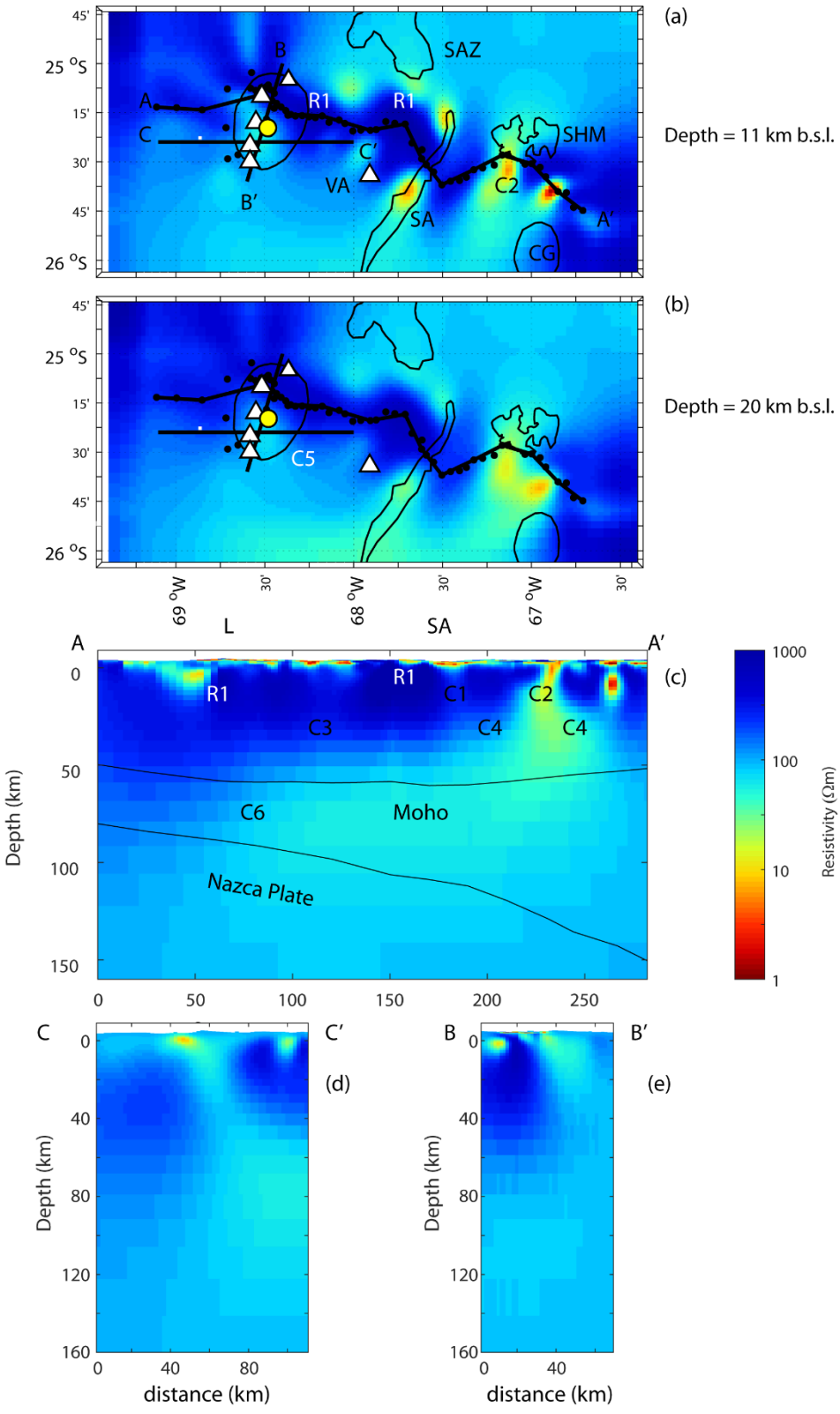

Figure S5(d) : Inversion model *puna_lazufre_8a* obtained by inversion of impedance and tipper data. Starting model was 100 Ωm.

4. Sensitivity tests

4.1 Sensitivity to resistivity below a specified depth

In the first set of edits, the model was made resistive below a specified depth and the results are illustrated in Figure S6 and summarized in Table S3. Changing the model below 50 km produced a relatively small change in overall misfit at frequencies less than 0.001 Hz. When the model was changed at depth of 40 km or shallower, a significant change in misfit occurred. All of the above model editing exercises used a statistical approach to determine if the change in misfit was significant using the method described by Lee et al., (2020).

			r.m.s. misfit		
Name	Region edited	resistivity	impedance	tipper	Overall
Puna_lazufre_60a			1.54	1.72	1.60
Puna_lazufre_60a_edit1	z > 50 km	1000 Ωm	2.02	1.81	1.95
Puna_lazufre_60a_edit2	z > 40 km	1000 Ωm	2.50	1.88	2.32
Puna_lazufre_60a_edit3	z > 30 km	1000 Ωm	3.25	1.99	2.92
Puna_lazufre_60a_edit4	z > 20 km	1000 Ωm	5.64	2.29	4.84
Puna_lazufre_60a_edit5	z > 10 km	1000 Ωm	9.12	2.87	7.72

Table S3 : Summary of sensitivity tests presented in Figure S6.

4.2 Sensitivity to model feature C5

In a second set of tests, feature C5 was made resistive and this is illustrated in Figure S7. The removal of feature C5 produces a significant change, especially in the region of high ϕ_{yx} values at frequencies less than 0.01 Hz and located east of Lazufre. This is as expected for an east-west oriented conductor that will primarily have a response in the yx component of the impedances, since the east-west electric currents will be strongest in an east-west oriented conductor.

			r.m.s. misfit		
Name	Region edited	resistivity	impedance	tipper	Overall
Puna_lazufre_60a			1.54	1.72	1.60
Puna_lazufre_60a_edit10	z = 5 to 30 km 68.6°W to 68°W 25.5°S to 25.25°S	100 Ωm	1.74	1.79	1.75

Table S4 : Resolution test for model feature C5

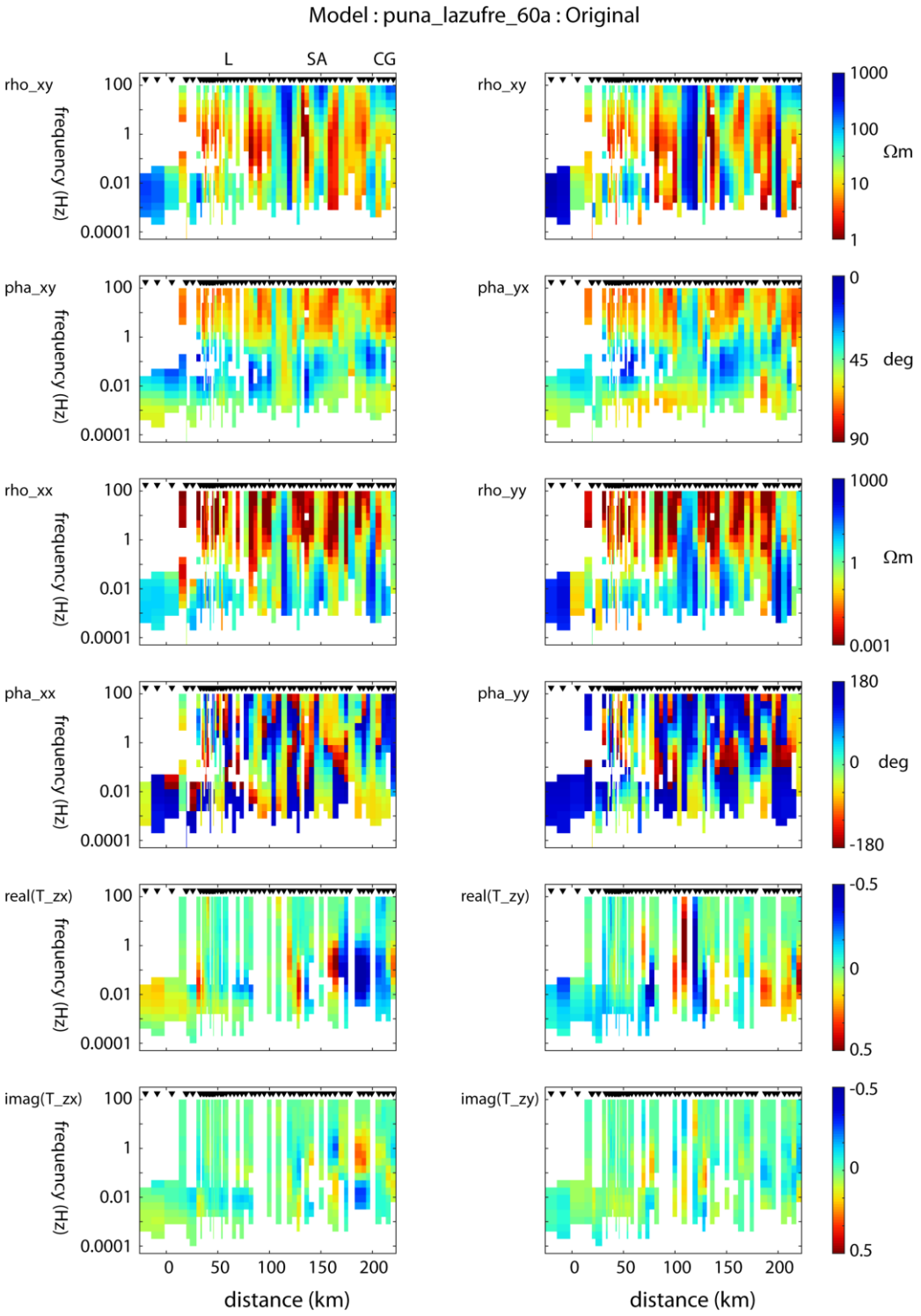

Figure S6(a) : Predicted data for the unedited inversion model *puna_lazufre_60a*.

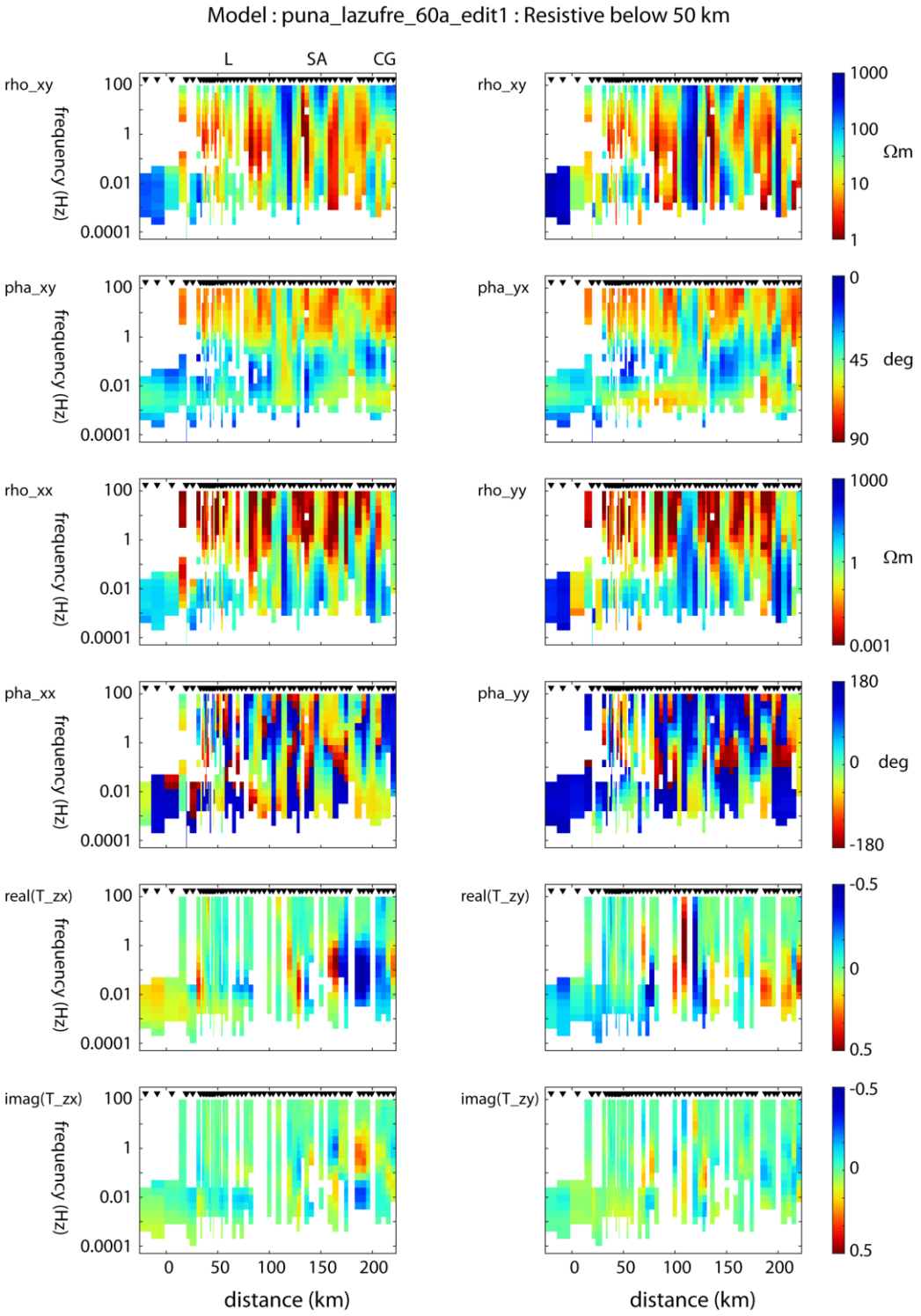

Figure S6(b) : Forward response of edited model *puna_lazufre_60a* with model replaced by a 1000 Ωm beginning at a depth of **50 km**.

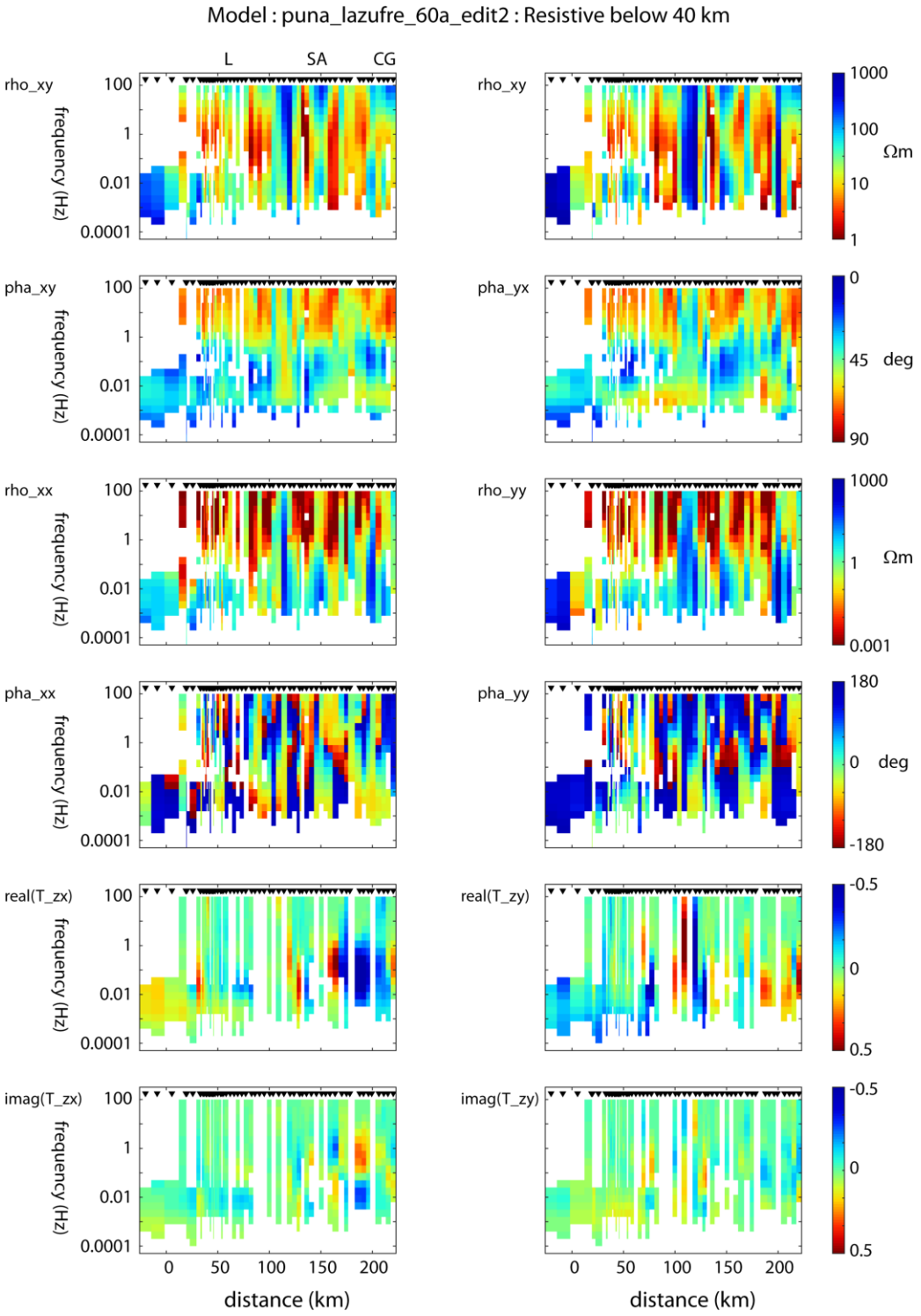

Figure S6(c) : Forward response of edited model *puna_lazufre_60a* with model replaced by a 1000 Ωm beginning at a depth of **40 km**.

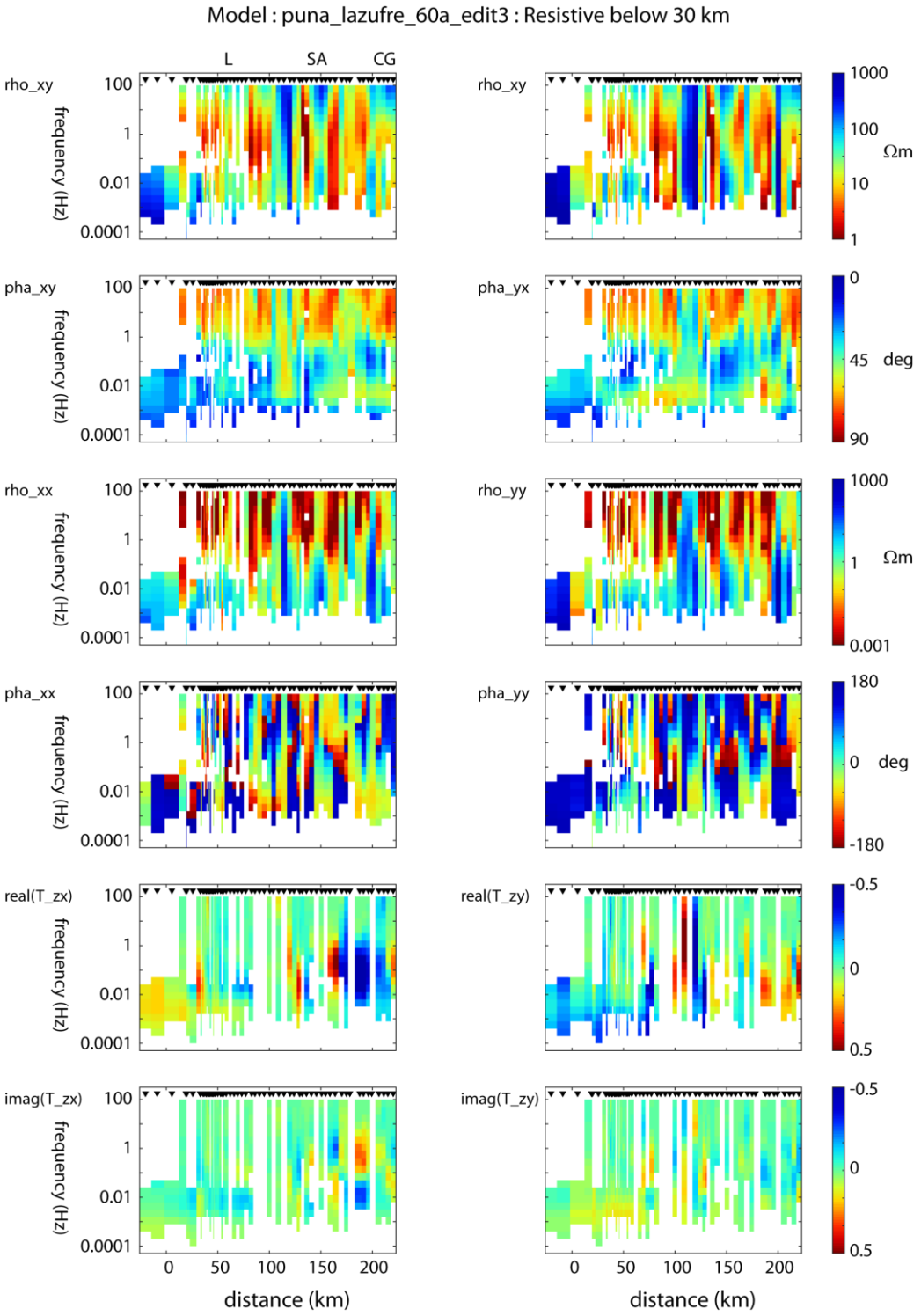

Figure S6(d) : Forward response of edited model *puna_lazufre_60a* with model replaced by a 1000 Ωm beginning at a depth of **30 km**.

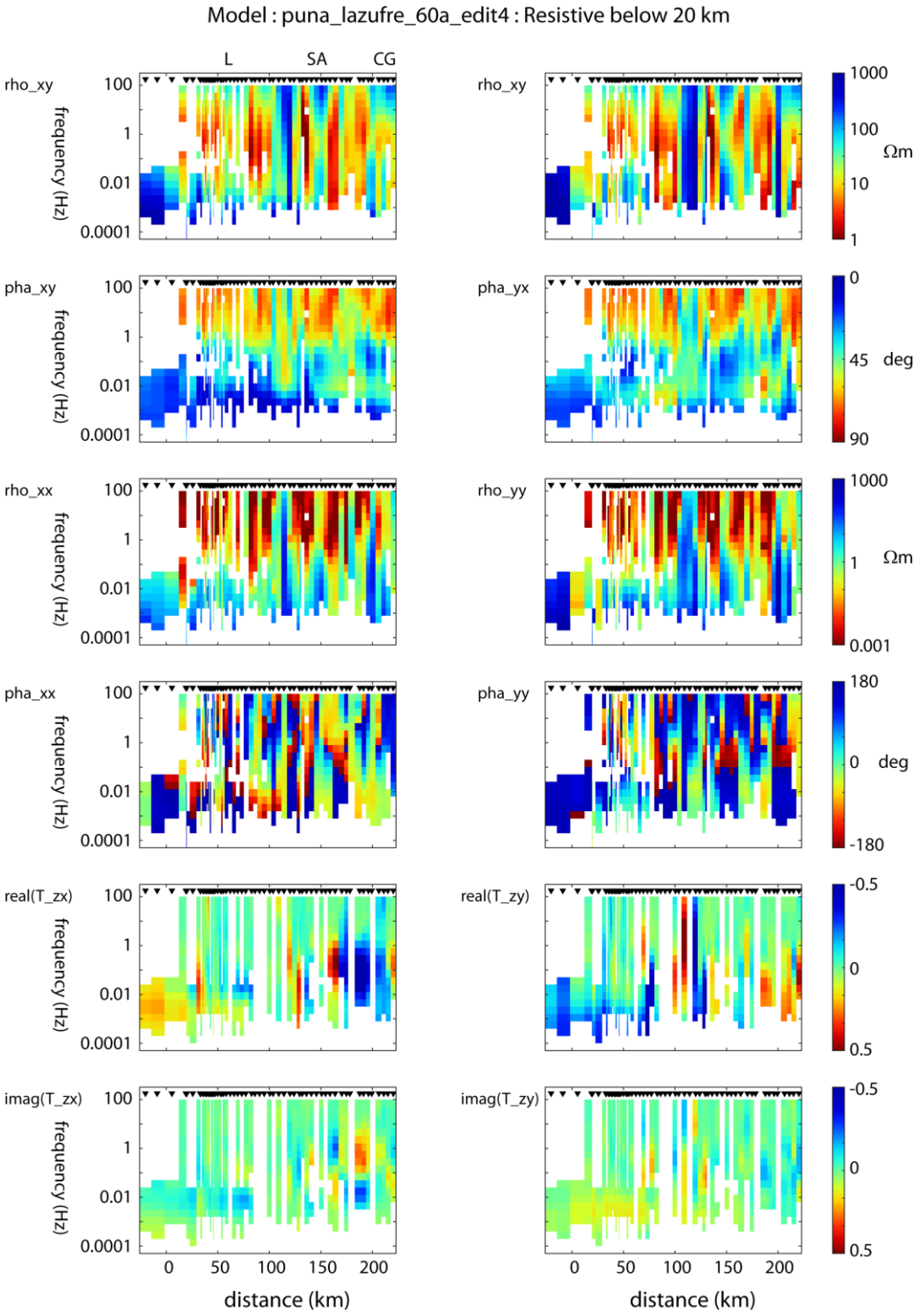

Figure S6(e) : Forward response of edited model *puna_lazufre_60a* with model replaced by a 1000 Ωm beginning at a depth of **20 km**.

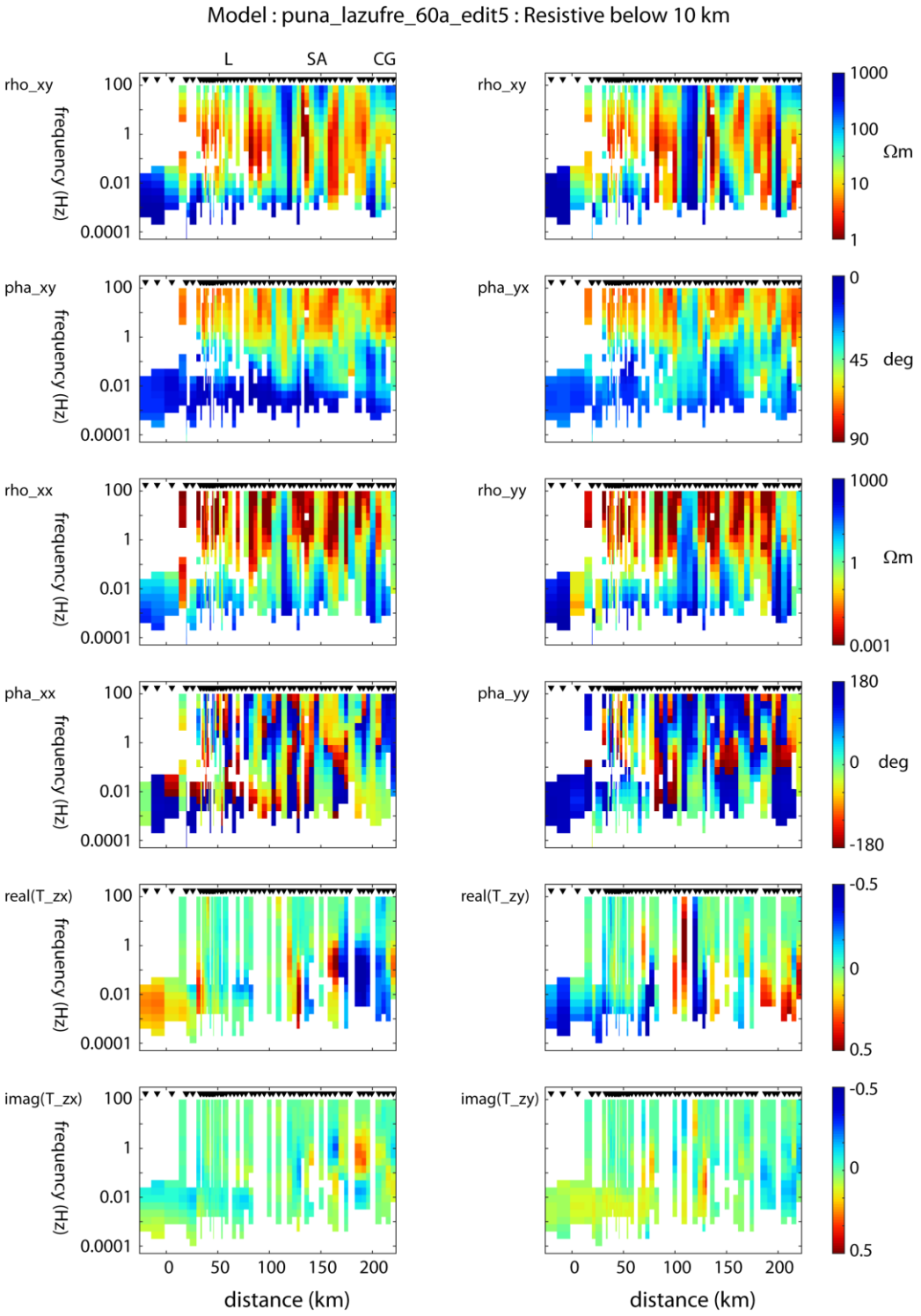

Figure S6(f) : Forward response of edited model *puna_lazufre_60a* with model replaced by a 1000 Ωm beginning at a depth of **10 km**.

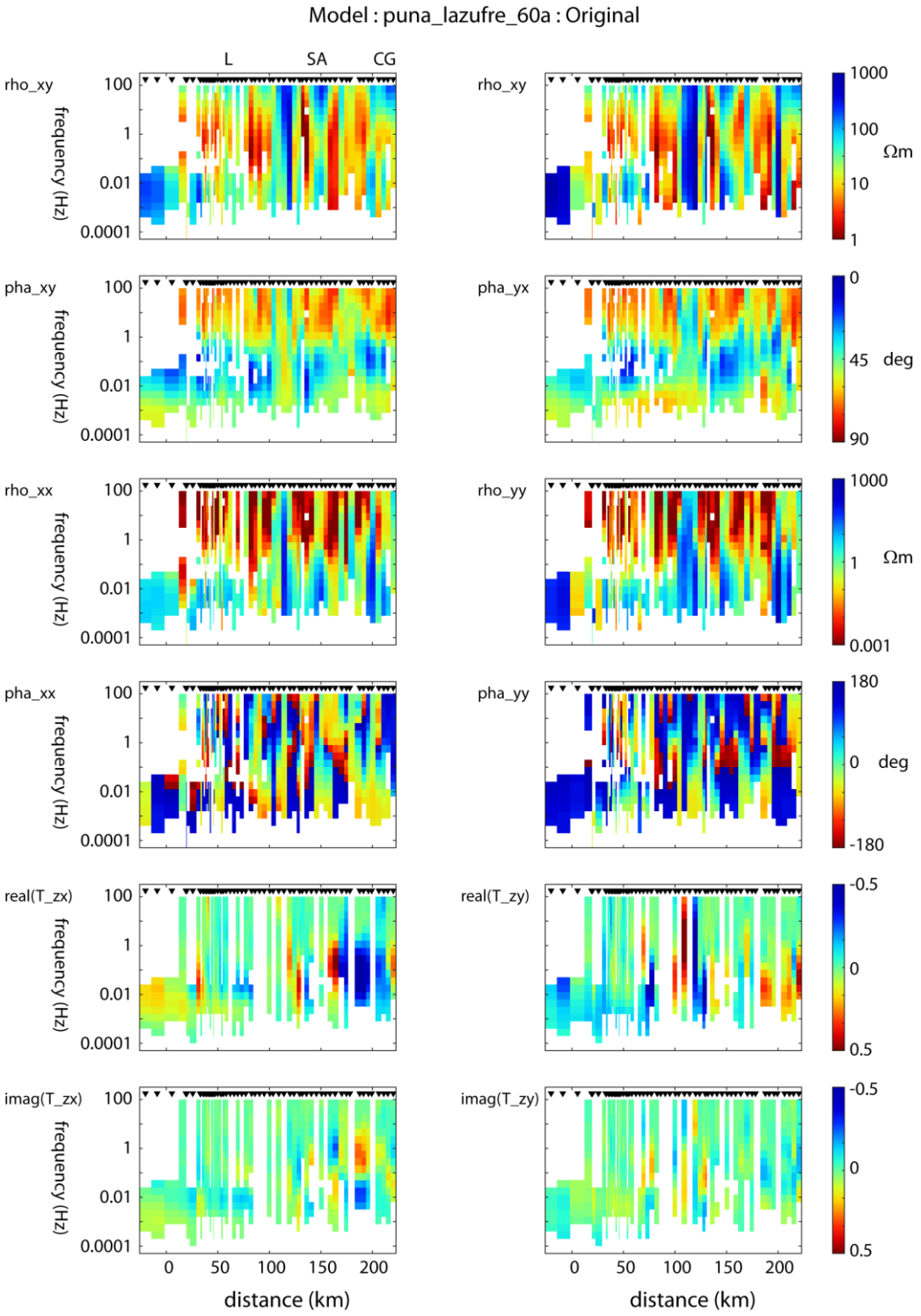

Figure S7(a) : Predicted data for the unedited inversion model *puna_lazufre_60a*.

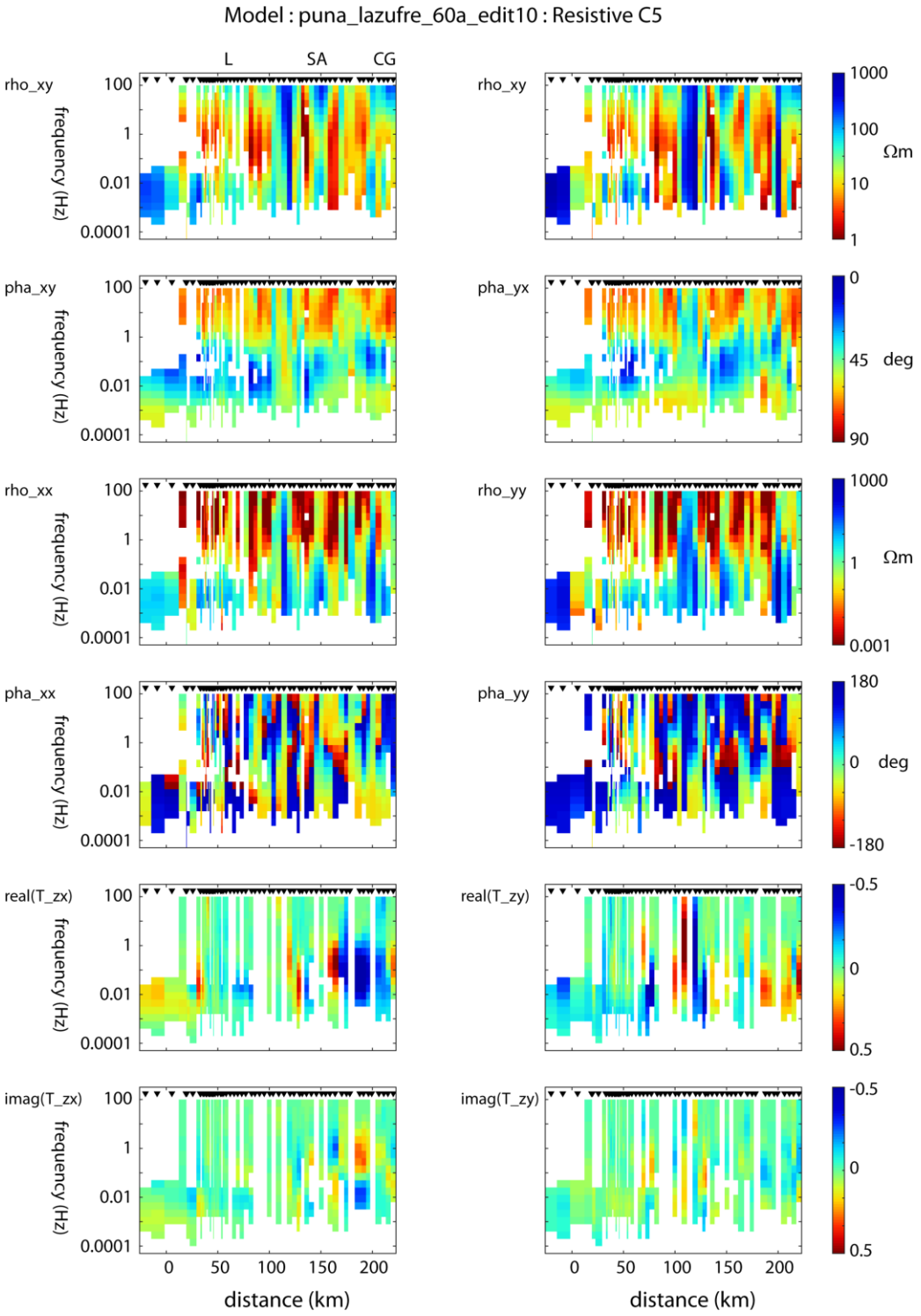

Figure S7(b) : Forward response of edited model *puna_lazufre_60a* with resistivity of model feature C5 set to 100 Ωm.

5. Synthetic MT inversions

The inversion models were further investigated using a synthetic inversion approach. A range of synthetic models were considered and representative results are presented in Figure S8.

Model *syn2* is characterized by a 30 Ωm crust, a 10 Ωm mantle wedge and a 1000 Ωm Nazca Plate. Within the crust, two conductive prisms with resistivity 1 Ωm were added to represent the two conductors detected in the field MT data inversion shown in Figures 6 and 7. These features correspond to the Lazufre Anomaly (LA) and Cerro Galan Anomaly (CGA) reported in the seismic study of Ward et al., (2017) and Bianchi et al., (2013). The synthetic model includes topography. Synthetic MT data were generated and Gaussian noise added at the 5% level. The synthetic data were then inverted using the same approach as for the field MT data and the results are shown in Figure S8(a) and S8(b). A synthetic inversion (*puna_lazufre_syn2_14*) began from a 10 Ωm halfspace, and converged with a damping factor of $\lambda = 10^{-8}$ after 100 iterations to a final r.m.s. misfit of 1.11.

The two crustal conductors are well imaged in the vertical sections. The resistive Nazca plate was not imaged, but this is as expected based on the model editing shown in Figure S6. In map view, it can be seen that the north-south extent of the conductors in the inversion models is limited by the spatial extent of the data.

Model *syn4* is illustrated in Figure S8(c) and Figure S8(d) and is identical to model *syn2*, except for the addition of a conductor to represent feature C5 in the models shown in Figures 6 and 7. A synthetic inversion (*puna_lazufre_syn4_14*) began from a 10 Ωm half-space, and converged with a damping factor of $\lambda = 10^{-8}$ after 103 iterations to a final r.m.s. misfit of 1.05. The synthetic inversion for *syn4* shows that this feature is resolved by existing data coverage, and can be seen to have an eastward dip.

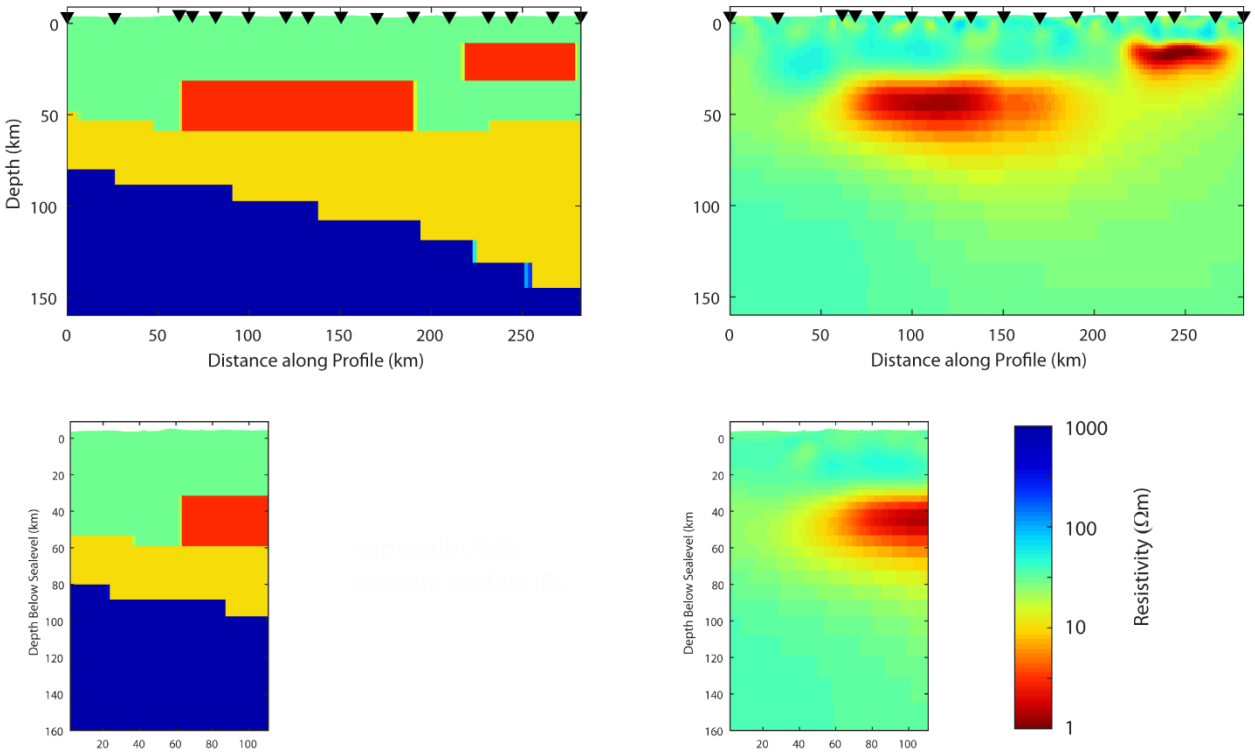

Figure S8(a) : Synthetic inversion test (syn2) used to investigate the resolution of the 3-D resistivity models presented in this study. The true model is shown in the left-hand column and contains 2-D conductors that strike north-south. One is located east of Lazufre and the other beneath Cerro Galan to represent the main features of the model presented in Figures 6 and 7. The true model contained an eastward dipping resistive feature that represents the Nazca Plate. The synthetic data has 5% noise added to the impedance and 0.02 added to the tipper. Forward model was plotted with script syn2_fwd_plot.m and the inverse model was plotted with S3D_v1.m

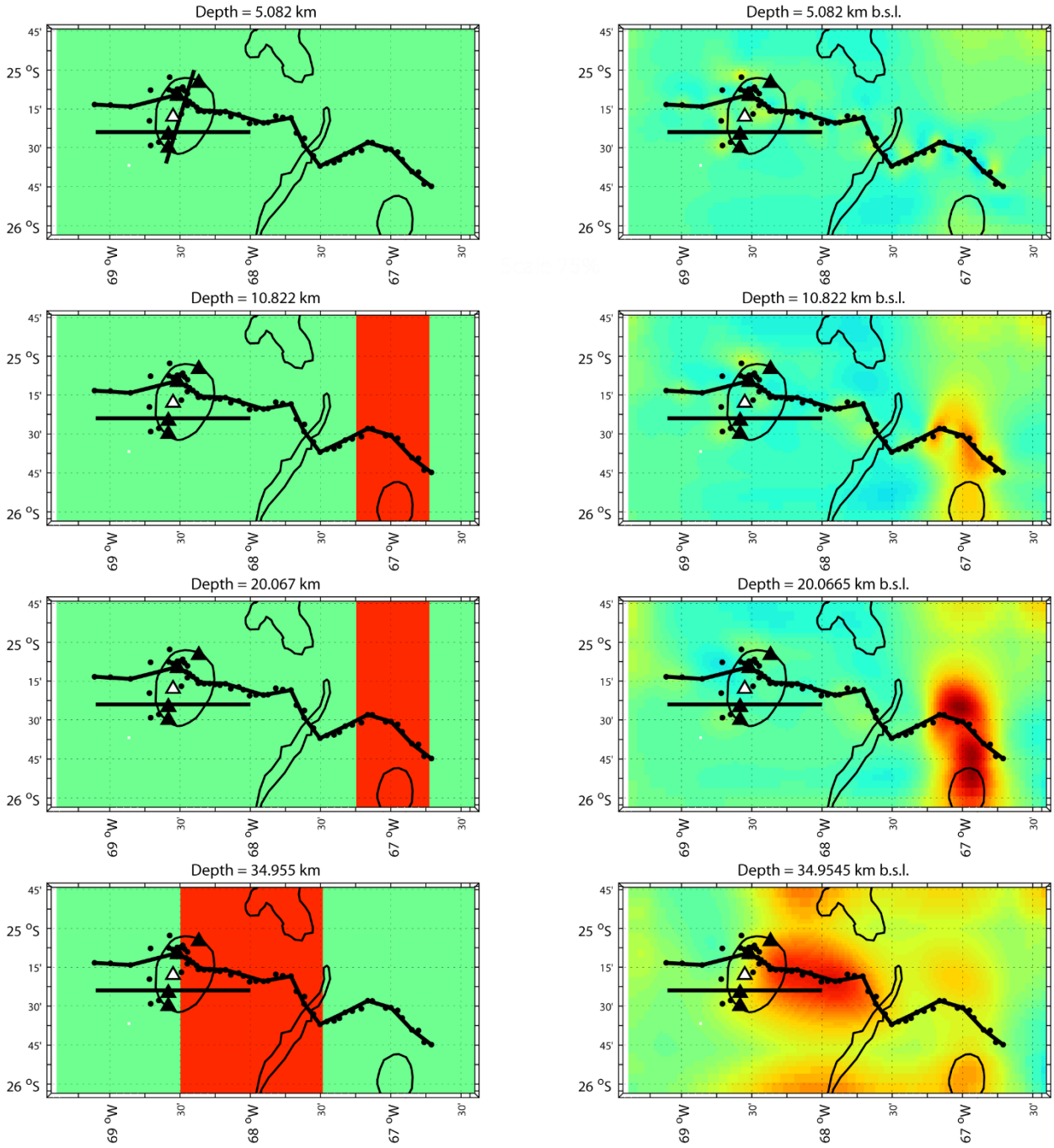

Figure S8(b) : As previous figure, but showing the true model and inversion model in plan view at depths of 5, 11, 20 and 35 km. Note that the two conductors are recovered at the correct depths beneath the line of MT stations. Away from the profile of MT stations the conductors are not imaged as expected. The resistive Nazca plate is not imaged in the inversion. The colour scale is the same as in Figure 8(a). The forward model was plotted with script syn2_fwd_plot.m and the inverse model plotted with S3D_v1.m

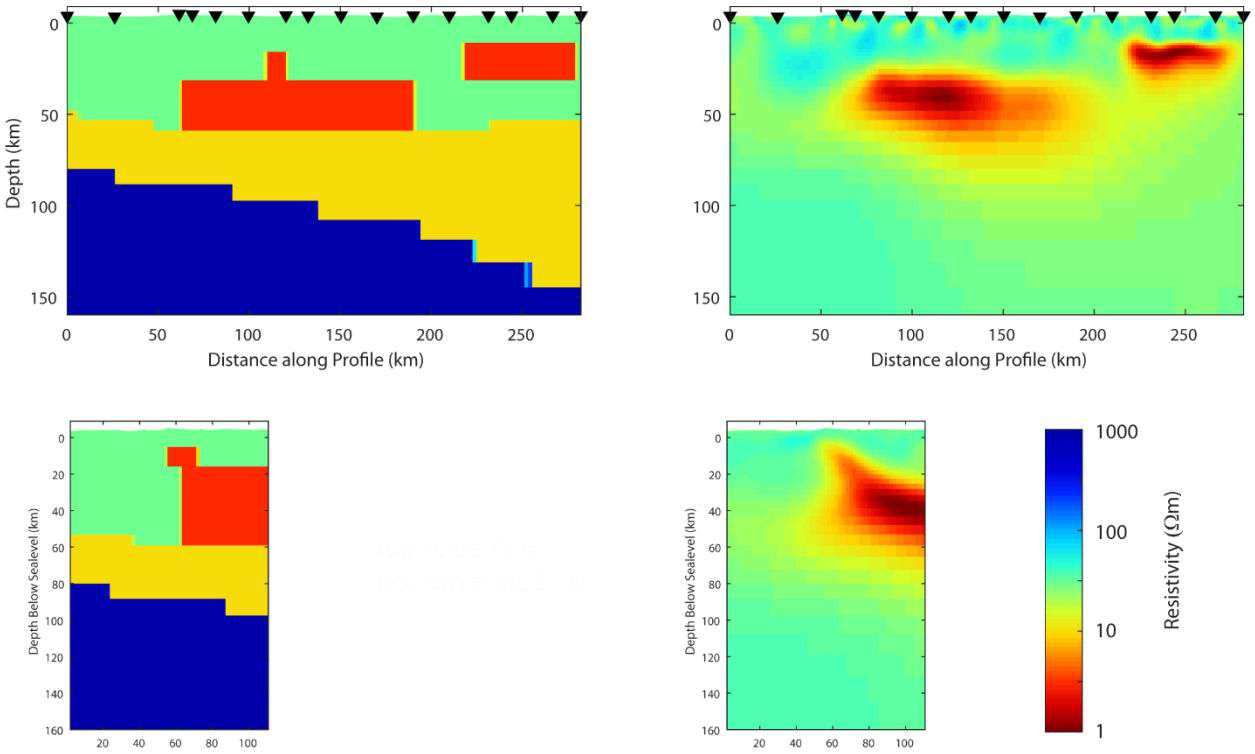

Figure S8(c) : Synthetic inversion test (syn4) used to investigate the resolution of the 3-D resistivity models presented in this study. The difference with syn2 is that a third conductor has been added which rises to the inflation centre from the western conductor. The true model contained a dipping resistive feature that represents the Nazca Plate. The synthetic data has 5% noise added to the impedance and 0.02 added to the tipper. The forward model was plotted with script syn4_fwd_plot.m and the inverse model was plotted with S3D_v1.m

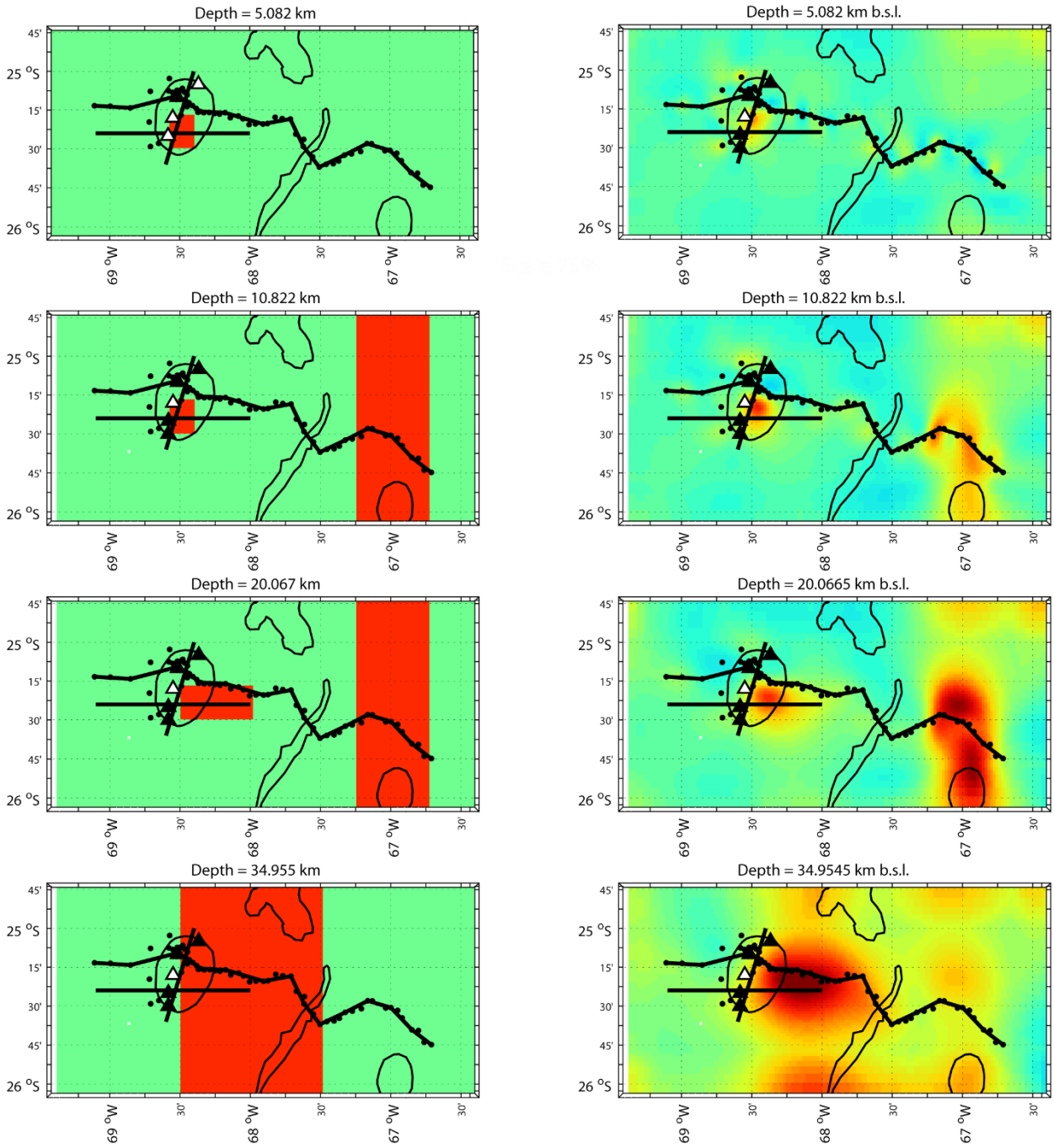

Figure S8(d) : As the previous figure, but showing the true model and inversion model in plan view at depths of 5, 11, 20 and 35 km. Note that the two conductors are recovered at the correct depths beneath the line of MT stations. Away from the profile of MT stations the conductors are not imaged as expected. The resistive Nazca plate is not imaged in the inversion. The colour scale is the same as in Figure 8(a) and (c). The forward model was plotted with script syn4_fwd_plot.m and the inverse model was plotted with S3D_v1.m